IJMMM International Journal of Minerals, Metallurgy and Materials 矿物冶金与材料学报（英文版）

Effect of bipolar-plates design on corrosion, mass and heat transfer in proton-exchange membrane fuel cells and water electrolyzers: A review

Jiuhong Zhang, Xiejing Luo, Yingyu Ding, Luqi Chang, and Chaofang Dong

Cite this article as:
Jiuhong Zhang, Xiejing Luo, Yingyu Ding, Luqi Chang, and Chaofang Dong, Effect of bipolar-plates design on corrosion, mass and heat transfer in proton-exchange membrane fuel cells and water electrolyzers: A review, *Int. J. Miner. Metall. Mater.*, 31(2024), No. 7, pp. 1599-1616. https://doi.org/10.1007/s12613-023-2803-6

View the article online at SpringerLink or IJMMM Webpage.

INTERNATIONAL JOURNAL OF
Minerals, Metallurgy and Materials

Volume 31, Number 7, July 2024
Page 1599

Invited Review

https://doi.org/10.1007/s12613-023-2803-6

Effect of bipolar-plates design on corrosion, mass and heat transfer in proton-exchange membrane fuel cells and water electrolyzers: A review

Jiuhong Zhang[1,2], *Xiejing Luo*[1,2], *Yingyu Ding*[1,2], *Luqi Chang*[1,2], *and Chaofang Dong*[1,2)✉]

1) Key Laboratory for Corrosion and Protection (MOE), Institute for Advanced Materials and Technology, University of Science and Technology Beijing, Beijing 100083, China

2) Beijing Advanced Innovation Center for Materials Genome Engineering, Beijing 100083, China

(Received: 15 August 2023; revised: 29 November 2023; accepted: 30 November 2023)

Abstract: Attaining a decarbonized and sustainable energy system, which is the core solution to global energy issues, is accessible through the development of hydrogen energy. Proton-exchange membrane water electrolyzers (PEMWEs) are promising devices for hydrogen production, given their high efficiency, rapid responsiveness, and compactness. Bipolar plates account for a relatively high percentage of the total cost and weight compared with other components of PEMWEs. Thus, optimization of their design may accelerate the promotion of PEMWEs. This paper reviews the advances in materials and flow-field design for bipolar plates. First, the working conditions of proton-exchange membrane fuel cells (PEMFCs) and PEMWEs are compared, including reaction direction, operating temperature, pressure, input/output, and potential. Then, the current research status of bipolar-plate substrates and surface coatings is summarized, and some typical channel-rib flow fields and porous flow fields are presented. Furthermore, the effects of materials on mass and heat transfer and the possibility of reducing corrosion by improving the flow field structure are explored. Finally, this review discusses the potential directions of the development of bipolar-plate design, including material fabrication, flow-field geometry optimization using three-dimensional printing, and surface-coating composition optimization based on computational materials science.

Keywords: bipolar-plates; flow design; mass and heat transfer; corrosion; water electrolyzers; fuel cells

1. Introduction

Hydrogen energy is a secure, economical, and nonpolluting energy source. Since the 1990s, hydrogen energy has been considered a critical and indispensable element of a decarbonized, sustainable energy system [1]. The complete process of obtaining hydrogen energy is usually divided into three steps: energy conversion, transportation, and storage [2]. To date, 96% of hydrogen production capacity is "gray hydrogen" from fossil fuels, and carbon-free "green hydrogen" production can be fulfilled by inputting renewable energy sources in electrolyzing water systems. The current situation of green hydrogen production being more expensive than gray hydrogen production will change as the cost of renewable energy decreases and electrolyzers become more cost-effective [3–4].

The current commercial water electrolysis technology is performed below 100°C. Two types of commercial electrolyzers are used in the industry: alkaline water electrolyzers and proton-exchange membrane water electrolyzers (PEMWEs) [5]. Alkaline electrolyzer technology is more mature and cheaper than that of PEMWEs but performs poorly at fluctuating potentials and high-power densities [6]. By contrast, PEMWEs can compensate for the disadvantages of alkaline electrolyzers. The improvement of the cost-performance ratio is critical to promoting PEMWEs technology in the long term.

Fig. 1 schematically shows the basic working principle of PEMWEs and proton-exchange membrane fuel cells (PEMFCs). Since they have a similar structure, the following is presented as an example of PEMWEs only. The physicochemical processes occurring inside PEMWEs in their operating state mainly include reactant transport, electrochemical reactions, proton and electron conduction, product elimination, heat generation, and heat dissipation. PEMWEs are assembled from bipolar plates and membrane electrode assembly (MEA). A MEA contains cathode/anode porous diffusion layers, cathode/anode catalytic layers, and a proton-exchange membrane. The general MEA possesses a symmetrical structure with the membrane as the axis. Bipolar plates perform prominent functions, including facilitating gas and liquid flow, providing structural support for MEAs, and conducting electric currents. For PEMWE stacks, the bipolar-plate weight is approximately 70% of the total weight and the bipolar-plate costs around 50% of the remaining expenses excluding membranes and catalysts [7]. Developers aim to improve several property parameters to meet the demand for performance optimization of bipolar plates; such parameters

✉ Corresponding author: Chaofang Dong E-mail: cfdong@ustb.edu.cn

include interfacial contact resistance (ICR) [8–10], thermal conductivity [11], electrical conductivity [12–14], mass transfer capability [15–18], and corrosion resistance [19–21]. The U.S. Department of Energy (DOE) proposed a development plan for the bipolar-plate technology applied in PEMFCs [22–23]. The plan mainly requires a bipolar-plate ICR below 10 $m\Omega \cdot cm^2$ and a corrosion current density below 1 $\mu A \cdot cm^{-2}$ in 2025 [24]. Designing excellent bipolar plates requires detailed investigation into several key aspects: a structural design that has a decisive effect on hydrothermal management, material selection that assures corrosion resistance at high potentials, and cost containment.

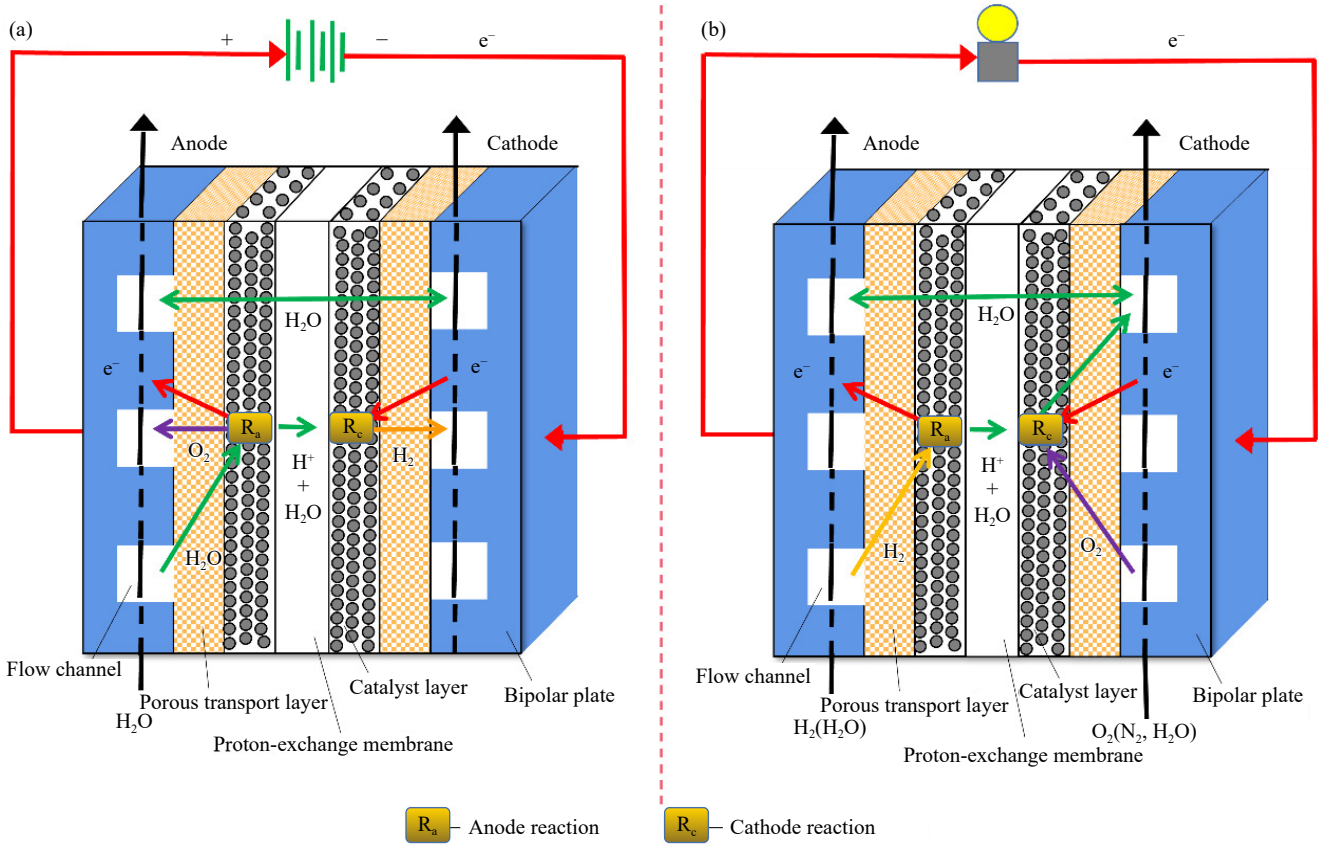

Fig. 1. Schematic of the basic working principle of (a) PEMWEs system and (b) PEMFCs system.

PEMWEs and PEMFCs have similar structures. However, their bipolar plates are not directly interchangeable. In PEMWEs, the decomposition of water into hydrogen and oxygen occurs when an electric current pass through the electrolyte; in PEMFCs, the reaction of hydrogen and oxygen generates electrical energy [25]. Different work environments and electrochemical conditions impose distinctive requirements on bipolar-plate design. In addition, material and flow-field design need to be coordinated in bipolar-plate design to ensure the compatibility between materials and flow fields and optimize the performance and efficiency of PEMWEs and PEMFCs. In this regard, the corrosion resistance and conductivity of materials and the uniformity and flow characteristics of the flow field must be considered.

The increasing prevalence of the concept of low carbon brought into sharp focus the design work of bipolar plates, which serve as key components of PEMWEs. Although separate reviews of bipolar plates for PEMWEs and PEMFCs have been published, those that compared the operating principles and design requirements are a few. Meanwhile, no study has analyzed the interaction of material selection and flow-field design in bipolar-plate design. Hereinto, this paper reviews the research progress of bipolar-plate design based on previous studies in terms of material selection and flow-field design. Substrates and coatings are presented for material selection, and traditional channel-rib flow fields, porous flow fields, and other novel structures for structural design are presented. In addition, analysis is conducted on the differences in service conditions between PEMWEs and PEMFCs bipolar plates and the potential interaction between material selection and flow-field design. This review aims to provide guidance to material and fluid engineers involved in bipolar-plate design.

2. Differences in working conditions of PEMWEs and PEMFCs

PEMWEs and PEMFCs exhibit a structural similarity that can be attributed to their similar composition and not only to their same membrane technology design. These devices have symmetrical structures with a membrane as the axis, and both consist of a membrane electrode and two bipolar plates. However, the components used for PEMFCs cannot be used directly on PEMWEs given their different service conditions,

including reaction direction, operating temperature, pressure, input/output, and potential.

(1) Reaction direction.

Differences in service conditions stem from the various internal reactions. PEMWEs utilize electrical energy to split water into oxygen and hydrogen. This reaction absorbs heat, which ultimately produces hydrogen [26–27]. Although PEMFCs convert hydrogen and oxygen into electrical energy and water, the reaction is exothermic. The ultimate goal of this process is to generate electricity [28].

(2) Operating temperature.

PEMWEs typically operate at low temperatures of around 50–80°C [29–30], and PEMFCs can operate at higher temperatures of around 80–120°C [31–32]. A high operating temperature allows PEMFCs to operate efficiently and induce fast reaction rates. Although studies have been conducted on the operation of high-temperature PEMWEs, the commercialization of this technology remains distant [33–34].

(3) Pressure.

A single PEMWE requires atmospheric pressure under average operating conditions [35–36], whereas an efficient single PEMFC preferably operates at a pressurized environment of 1×10^6–3×10^6 Pa [37–39]. As for commercial products, the increased operating pressure is inevitably introduced in multiple cell integrations of PEMWEs and PEMFCs. The delivery pressure of PEMWE stacks from Nel Company in Norway is between 1.38×10^7 and 3×10^7 Pa, depending on the rate of hydrogen production.

(4) Input and output.

Most of the current PEMWEs and PEMFCs operate at temperatures below 100°C, and thus, the water inside them mainly exists in liquid form. The PEMWE inlet is all liquid water, and the PEMFC inlet is all gas. Both exclude the two-phase flow at the outlet [40–41]. The increase in flow rate guarantees the reactant supply for electrochemical reactions in the catalytic layers. However, evident wastage is subsequently produced as some reactants are expelled from the outlet before they can react. The inlet of PEMFCs exhibits a lower flow rate compared with that of PEMWEs due to economic and safety considerations for hydrogen [42–45].

(5) Potential.

The potential difference in bipolar plates of PEMWEs is consistently higher compared with that of PEMFCs. PEMFC bipolar plates have potential in the range of 0.2–1 V [46–48]. The PEMWE electrolysis reaction involves a critical theoretical potential of 1.23 V [7]. The improvement of hydrogen production capacity can be attained by further increasing the electrolysis potential. Consequently, the increased demand for the durability of bipolar plates at high potential has been proposed in terms of PEMWE development.

Bipolar-plate products for PEMFCs cannot be used directly on PEMWEs. Although information can be obtained from the PEMFC bipolar-plate design, unresolved issues that require the attention of research and development staff remain. In comparison with PEMFCs, PEMWEs are evolving toward higher potentials and larger sizes, which present challenges in terms of manufacturing processes and flow-field design for larger-scale applications.

3. Types of materials

3.1. Base materials

The widely used graphite bipolar plates are made of composite materials consisting mainly of graphite flakes and resin binder. They possess good electrical conductivity, corrosion resistance, and dimensional stability. However, their limitations lie in their mechanical strength, surface finish, and operating temperature range. On the other hand, metal bipolar plates have gained considerable attention as an alternative to graphite plates. These materials are usually made of stainless steel (SS), titanium, or other metal alloys and are manufactured through various processes, such as stamping, machining, or electroforming. Compared with graphite plates, metal plates offer higher mechanical strength and robustness and better temperature resistance. These advantages have led to a growing interest in metal bipolar plates for fuel-cell applications [7].

3.1.1. Graphite bipolar plates

The manufacturing process of graphite bipolar plates becomes complicated in batch manufacturing; however, graphite bipolar plates remain more convenient to use in new flow-field verification process than metal bipolar plates that require die stamping [49]. This application is one of the reasons why high-density graphite has been used in bipolar plates for the longest time. In addition, the inherent properties of graphite materials, such as their excellent electrical conductivity and corrosion resistance, significantly contribute to their performance. With the increased demand for PEMWE working conditions, pure graphite plates can no longer meet the service requirements. At 1.8 V, the oxidization of carbon produces carbon dioxide, which in turn leads to a gradual decrease in conductivity [50]. Based on the development of graphite plates, the proposed carbon-containing composite material is a feasible solution for applications in high potential environments. At this stage, the solution must address the issues of improving the binder conductivity, boosting the conductivity and corrosion resistance of fillers, and ensuring stability at high potentials. Given that bipolar plates operate in a stacked condition, a firm bond between the filler and the matrix is required. As shown in Fig. 2(a)–(b), graphite/graphene-filled polybenzoxazine composites possess good mechanical properties. The interior of aniline-based benzoxazine monomer (BA-a) resin exhibits a substantially low melt viscosity, which facilitates excellent wetting properties of the fillers. As a result, the filler and the matrix exhibit a robust interfacial adhesion. The performance of the composite material is also influenced by factors such as the filler particle size, filler aspect ratio, weight/volume ratio during mixing, and synergistic effect between different fillers [51–52]. Expanded graphite, with its good thermal conductivity, low density, low cost, and stability, is the ideal substrate compared with other carbon materials. The corrosion current density reaches 79.8 $\mu A \cdot cm^{-2}$ for expanded-graphite (EG) bipolar plates,

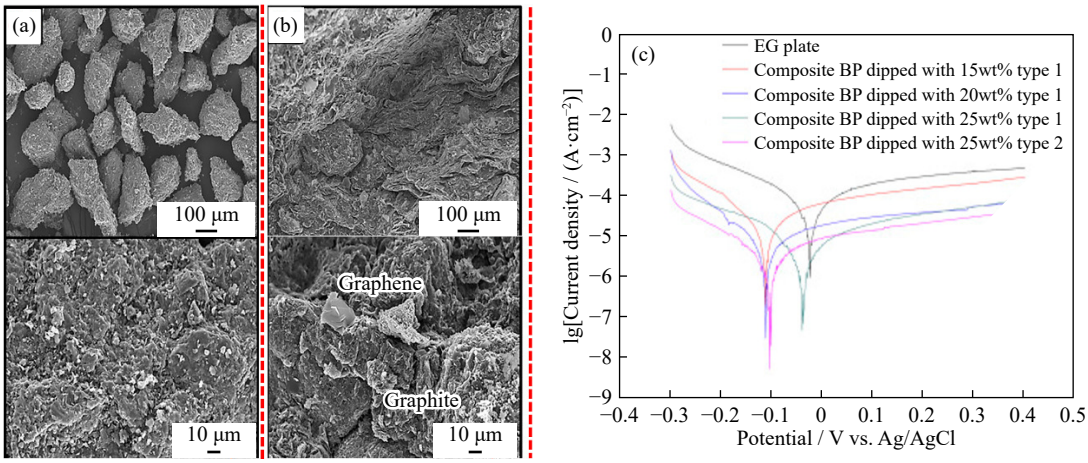

Fig. 2. SEM images of the fracture surface of (a) pure graphite and (b) 80.5wt%/2.5wt% graphite-/graphene-filled polybenzoxazine. M. Phuangngamphan, M. Okhawilai, S. Hiziroglu, and S. Rimdusit, *J. Appl. Polym. Sci.*, 136, e47183 (2019) [51]. Copyright Wiley-VCH Verlag GmbH & Co. KGaA. Reproduced with permission, and (c) potentiodynamic polarization curves of EG plates and EG/phenolic resin composite plates with different concentrations of resin solution. Reprinted from *Int. J. Hydrogen Energy*, 41, W.W. Li, S. Jing, S.B. Wang, C. Wang, and X.F. Xie, Experimental investigation of expanded graphite/phenolic resin composite bipolar plate, 16240, Copyright 2016, with permission from Elsevier.

which indicates that the upper limit of the performance for pure carbon materials did not satisfy the DOE 2025 requirements [53]. As displayed in Fig. 2(c), phenolic resins, as polymer fillers, considerably reduce corrosion current density by preventing intergranular corrosion.

3.1.2. Metal bipolar plates

Metallic materials ensure the long-term operation of bipolar plates under acidic conditions because the generation of a passivating film on the metal surface prevents further substrate dissolution [54]. However, the generation of passivating films increases the ICR and leads to an increased ohmic loss of the PEMWE system [55]. SS and titanium, which can generate passivate films, are currently the dominant materials used in metal bipolar plates.

SS bipolar plates have the advantages of excellent mechanical properties, good impact resistance, and low cost, and the disadvantages include high density and insufficient corrosion resistance at high potentials [56]. For the 316L SS bipolar plates in Fig. 3(a1), the contact angle of less than 90° indicates a hydrophilic surface [57]. As shown in Fig. 3(a2)–(a3), the corrosion current density and ICR at 150 $N \cdot cm^{-2}$ measured 7.643 $\mu A \cdot cm^{-2}$ and 44.29 $m\Omega \cdot cm^2$, respectively. The ICR of 316L SS is lower than that of graphite materials due to the difficult conduction of electricity through the metal passivate film (Table 1). Through the application of additive manufacturing techniques, the surface condition and structure of metal bipolar plates can be optimized to improve electrical conductivity and durability. The three-dimensional (3D)-printed 316L bipolar plates have ICR that comply with the requirement set by DOE, which is less than 10 $m\Omega \cdot cm^2$ [65]. Given the high density of dislocations in their microscopic cell structure, 3D-printed 316L SS bipolar plates can resist corrosion under hydrogen-rich conditions. Although positive enhancement of corrosion resistance is acquired in SS via 3D printing technology, such a result remains insufficient to meet the requirements of DOE 2025 on the corrosion current density [66].

Titanium and aluminum alloys are less dense than SS. Lightweight-alloy bipolar plates can be used to greatly reduce the weight of an entire stack. On the anode side of PEMWEs, the oxide film produced on the aluminum and titanium plates increases the ICR. Aluminum bipolar plates, which must be guaranteed to be 100% nonporous, have high coating requirements. Otherwise, the ionic conductivity will be affected when aluminum reaches the proton-exchange membrane after dissolution [67]. Compared with that obtained when using aluminum, the ICR produced via the oxidation of titanium surface is smaller, which ensures that titanium as a substrate is conductive and noncorrosive to a certain extent. Ti_4O_7 has an electrical conductivity of 1.0×10^5 $S \cdot m^{-1}$ [68]. Therefore, titanium-alloy bipolar plates have desirable prospects for application on the anode side of PEMWEs. However, titanium is prone to embrittlement in hydrogen-containing cathode environments [69]. For the TA1 bipolar plates in Fig. 3(b1), the contact angle of less than 90° indicates a hydrophilic surface. Shi *et al.* [58] considered the differences between cathodic and anodic conditions when measuring ICR and corrosion currents and observed that the material's performance was superior in the former case. As presented in Fig. 3(b2)–(b3), the corrosion current density in the simulated cathodic environment and the ICR at 140 $N \cdot cm^{-2}$ measured 1.084 $\mu A \cdot cm^{-2}$ and 176.9 $m\Omega \cdot cm^2$, respectively. The destruction of the passivate firm on the titanium surface resulted in the formation of unprotected titanium–fluoride compounds. Although TA1 exhibited a better corrosion current density than 316L SS, it still failed to meet the requirements of DOE 2025. Current metal materials cannot meet DOE requirements without considering surface treatment, except precious metal substrates that are not considered due to their high cost.

3.2. Coating materials

Developers have modified the metal substrate surface to ensure the prolonged service life of bipolar plates under work

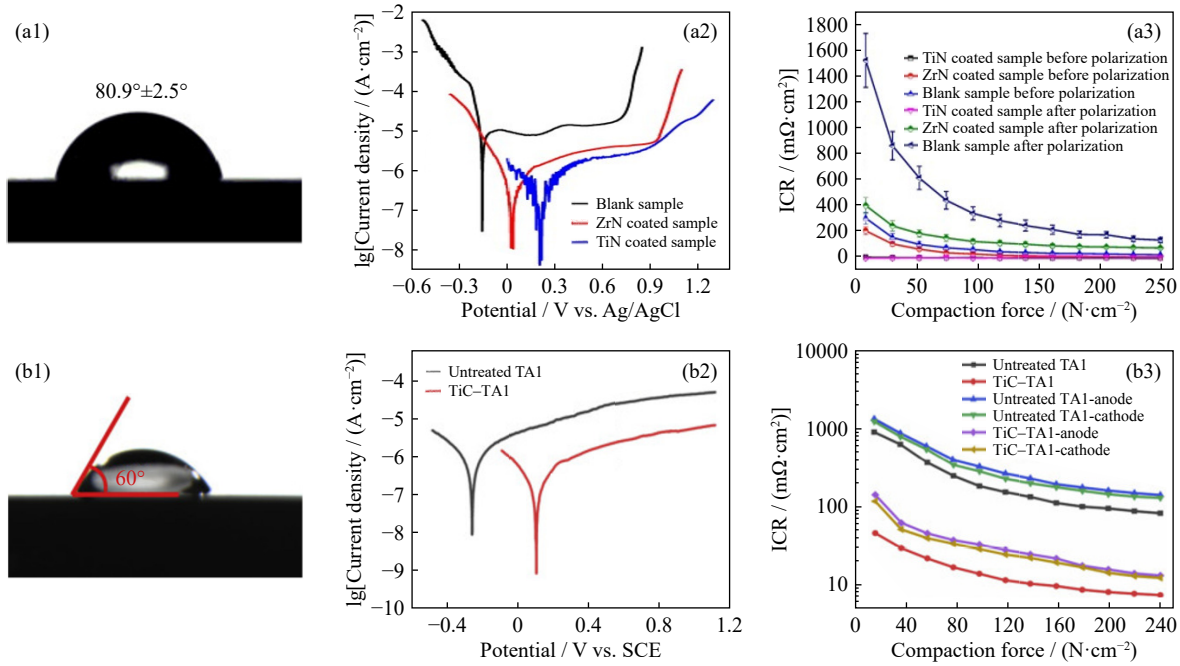

Fig. 3. Bipolar plates made of stainless steel and titanium in the simulated cathodic environment of a PEMFC: (a1) contact angle of the 316L SS; (a2) potentiodynamic polarization curve of the 316L SS; (a3) interfacial contact resistance of 316L SS. Reprinted from *Surf. Coat. Technol.*, 363, P. Yi, L.J. Zhu, C.F. Dong, and K. Xiao, Corrosion and interfacial contact resistance of 316L stainless steel coated with magnetron sputtered ZrN and TiN in the simulated cathodic environment of a proton-exchange membrane fuel cell, 198, Copyright 2019, with permission from Elsevier; (b1) contact angle of untreated TA1; (b2) potentiodynamic polarization curves of untreated TA1; (b3) interfacial contact resistance of TA1. Reprinted from *Int. J. Hydrogen Energy*, 45, J.F. Shi, P.C. Zhang, Y.T. Han, *et al.*, Investigation on electrochemical behavior and surface conductivity of titanium carbide modified Ti bipolar plate of PEMFC, 10050, Copyright 2020, with permission from Elsevier.

potential. The surface condition of bipolar plates can be affected by acidic, high-temperature, and hydrogen-rich or oxygen-rich conditions, which ultimately lead to increases in the corrosion current density and ICR. A minority of bipolar plates without surface treatment can meet the requirements of DOE 2025 [70]. Excellent surface treatment is required to simultaneously ensure corrosion resistance and improve the electrical conductivity of bipolar plates. Based on compositional differences, coatings on bipolar plates can be classified as metallic, carbon-based, and polymer coatings.

3.2.1. Metal and compound coatings

Metal coating materials include metal nitride, metal carbide, metal oxide, precious metal, and alloy coatings. Precious metals are chemically inert with good electrical conductivity [71]. Research has been conducted on 316L SS covered with Pt [72] and Au coatings [73]. However, the plating of metal monomers should be carried out carefully to avoid the unevenness of the substrate surface, which increases risk of localized corrosion. As shown in Fig. 4(a1), 3D-printed 316 L SS bipolar plates were coated with 1 μm gold layer after polishing treatment, which reduced the ICR to 6.4 mΩ·cm^2 at the pressure of 1.45 MPa [59]. As shown in Fig. 4(a2), the gold layer ensured the stable corrosion resistance of the substrate at high potentials but failed to meet the DOE requirements. Although precious metal coatings are extremely stable at high potentials, their high cost diminishes the feasibility of large-scale commercialization.

Initially, metal oxide coatings were formed directly on the surface of metal substrates, but their corrosion resistance and electrical conductivity were inadequate. The addition of Nb and Ta to TiO_2 can change a part of Ti^{4+} into Ti^{3+}, which improves the conductivity of TiO_2 coatings [74–75]. The Ti_4O_7 coating has an ICR of approximately 5 mΩ·cm^2, which is comparable to that of precious metal coatings [68]. Metal carbide coatings are not only relatively inexpensive to prepare but also form dense and uniform films on SS substrates. Carbide coatings exhibit good hydrophobicity at the interface of contact with the solution and strong bonding capability with the metal matrix, as shown in Fig. 4(b1) [60]. Metal nitrides feature excellent electrical conductivity and thermal stability. The investigation of TiN films on bipolar plates is still pending, concentrating on the effect of the preparation process on the coating microstructure. The use of unreasonable process parameters can lead to cratering defects on the surface of TiN films (Fig. 4(c1)) [61]. As displayed in Fig. 4 (b2) and (c2), nitride and carbide coatings meet the DOE 2025 requirements for corrosion current density. The two combinations of coatings and substrates have the best prospects for commercialization due to their high performance and simple structure (Table 1).

The coating surface must be uniform and smooth because a nonuniform surface may lead to defects and crevice corrosion. Nanocoatings have been proposed to fulfill the above requirements. These materials can effectively prevent corrosive ions from penetrating the metal substrate while ensuring good electrical conductivity. Tetrakis (dimethylamino) titani-

Table 1. Corrosion current density and ICR of the common base and coating materials applied in bipolar plates

Substrate	Coatings	Testing conditions	i_{corr} / ($\mu A \cdot cm^{-2}$)	ICR / ($m\Omega \cdot cm^2$)	Refs.
Graphite-/graphene-filled polybenzoxazine	—	—	—	3.52	[51]
EG	—	1 M H_2SO_4, 80°C	79.8	—	[53]
EG/phenolic resin composite	—		4	8.9	
316L SS	—	0.5 M H_2SO_4, 2×10^{-6} HF, 70°C	7.643	44.29	[57]
	TiN		0.099	1.544	
	ZrN		0.209	18.86	
TA1	—	0.5 M H_2SO_4, 2×10^{-6} HF, 70°C	1.084	176.9	[58]
	TiC		0.137	46.9	
AM 316L SS	—	pH = 2, H_2SO_4, 22°C	>1	22.3	[59]
	Au		>10	6.4	
316L SS	—	0.01 M H_2SO_4, 5×10^{-6} HF, 75°C	2.0	—	[60]
	CrN		0.4	—	
	CrC		0.5	—	
Bare Ti	—	0.5 M H_2SO_4, 2×10^{-6} HF, 70°C	3.34	35.0	[61]
	Ti–N		0.47	3.0	
316L SS	—	pH=5.5, H_2SO_4, 5×10^{-6} HF, 75°C	1.47	11.0	[62]
	Ti		3.79	4.8	
	TiN		145.3	5.0	
	CrN/TiN		15.04	5.8	
	Ti/TiN		139.43	10.0	
316L SS	Nanolayered TiC_x/a-C film	pH = 3, H_2SO_4, 0.1×10^{-6} HF, 80°C	<0.5	<3	[63]
316L SS	—	0.5 M H_2SO_4, 2×10^{-6} NaF, 80°C	35	—	[64]
	PAMT		3	—	
	PPY		25	—	
	PAMT on PPY		12	—	
	PPY on PAMT		39	—	

Notes: DOE requirement $i_{corr} < 1\ \mu A \cdot cm^{-2}$ and ICR < $10\ m\Omega \cdot cm^2$, PAMT represents poly(2-amino-5-mercapto-1,3,4- thiadiazole), PPY represents polypyrrole, and a-C film represents amorphous carbon film.

um-TiN thin films prepared through plasma-enhanced atomic layer deposition methods exhibited excellent corrosion resistance because the films formed on the 316L substrate surface were free of corrosive impurities or pinholes. At a compression force of 127 $N \cdot cm^{-2}$, the ICR was reduced successfully from 35.868 to 15.239 $m\Omega \cdot cm^2$ [76]. Dense, defect-free, and well-adhered nanocrystalline β-Nb_2N coatings were fabricated on a 430 ferritic SS. The ICR of bipolar plates with coatings was less than 10 $m\Omega \cdot cm^2$ after 500 h of potentiostatic polarization [77]. By employing a double-cathode glow discharge plasma technique, a novel electrically conductive Ta_2N nanoceramic coating was fabricated through reactive sputter deposition [78]. The coating's microstructure comprised fine equiaxed Ta_2N grains with an average grain size of 13 nm. Small grains mean a great number of grain boundaries, which not only causes difficulty for corrosive media to penetrate the coating but also allows for smooth electron transport within crystals. An identical technique was employed to fabricate ZrN thin films with a grain size of approximately 15 nm [79]. ZrN-coated bipolar plates maintained their electrical conductivity and corrosion resistance after 5 h of potentiostatic polarization. Meanwhile, MAX-phase material coatings have the electrical conductivity of metals and the durability of ceramics, such as Ti_2AlC [80].

Multilayer or composite coatings can be used to solve the problem of bipolar-plate durability under sudden potential changes due to start-stop conditions. Composite coatings can incorporate metal particles with excellent electrical conductivity. When 316L SS was used as the substrate, the Au/TiN composite coating demonstrated superior electrical conductivity and corrosion resistance than the standard TiN coating [81]. The improvement in the ICR was most pronounced at the Au surface coverage of 4%–6% [82]. Polytetrafluoroethylene (PTFE), carbon cloth, and Ag were selected for the multilayer coating on the Mg substrate, the corrosion current of 0.058 $\mu A \cdot cm^{-2}$ and ICR of 27.28 $m\Omega \cdot cm^2$ were measured at a pressure of 1.4 MPa. The PTFE material guaranteed that the coating had a smooth surface but reduced the electrical conductivity [83]. For the enhanced electrical conductivity of composite coatings, some researchers added C and TiN components to the PTFE surface [84].

Multilayer coatings are still dominated by metal oxides, metal carbides, and metal nitrides in combination with each other. Studies should investigate the optimal stacking order

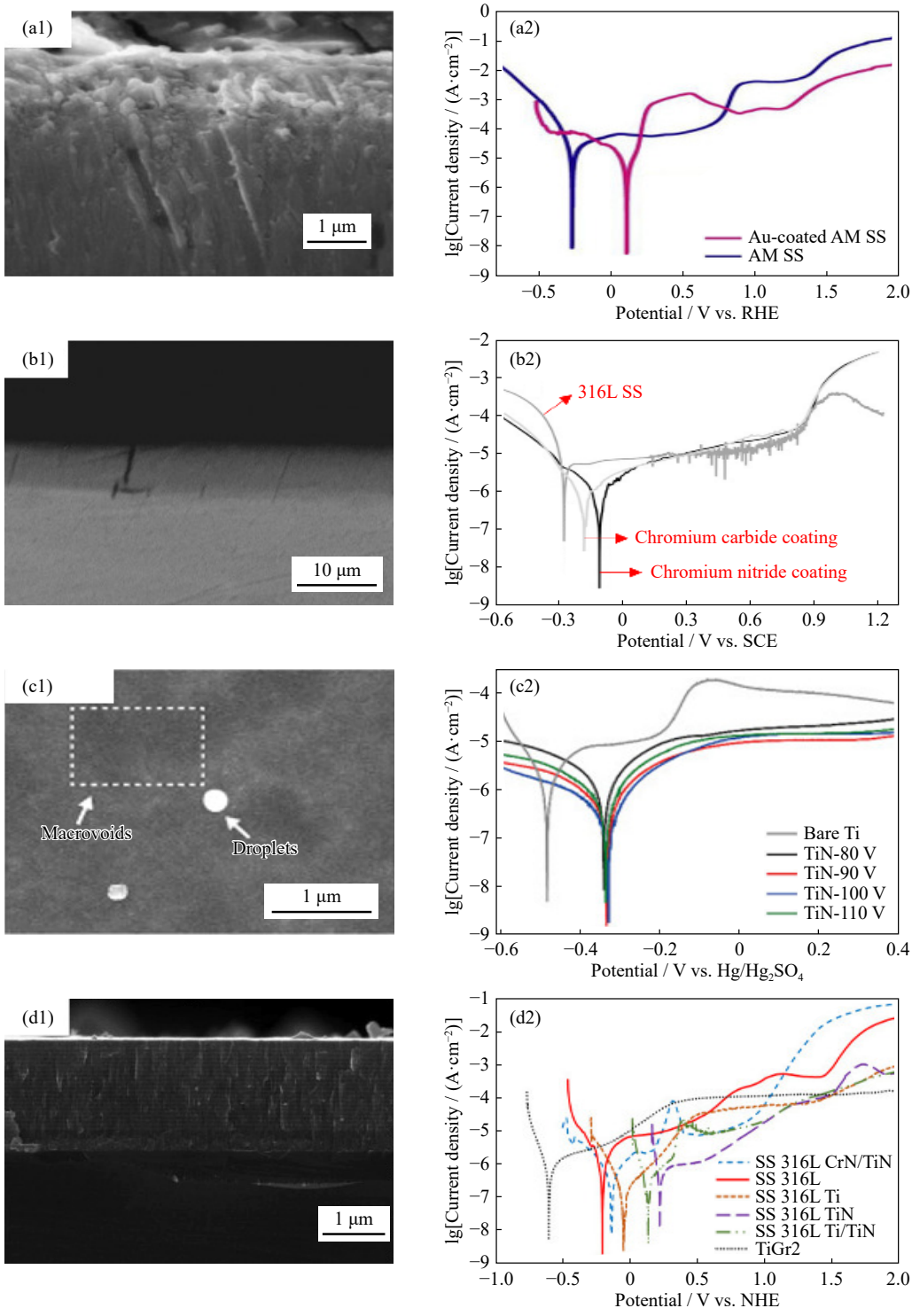

Fig. 4. SEM images and potentiodynamic polarization curves of precious metal, metal carbide, metal nitride, and multilayer coatings: (a1) SEM image revealing the cross-section of Au-coated AM SS bipolar plates; (a2) potentiodynamic polarization curves of AM SS bipolar plates with Au coating. Reprinted from *J. Power Sources*, 396, G.Q. Yang, S.L. Yu, J.K. Mo, *et al.*, Bipolar plate development with additive manufacturing and protective coating for durable and high-efficiency hydrogen production, 590, Copyright 2018, with permission from Elsevier; (b1) SEM image revealing the cross-section of chromium carbide coating; (b2) potentiodynamic polarization curves of 316L SS with carbide coating. H.H. Ghahfarokhi, A. Saatchi, and S.M. Monirvaghefi, *Fuel Cells*, 16, 356 (2016) [60]. Copyright Wiley-VCH Verlag GmbH & Co. KGaA. Reproduced with permission; (c1) SEM image revealing the surface of TiN-coated Ti; (c2) potentiodynamic polarization curves of TiN-coated Ti. Reprinted from *Int. J. Hydrogen Energy*, 46, T. Li, Z. Yan, Z.Z. Liu, Y.G. Yan, and Y.G. Chen, Surface microstructure and performance of TiN monolayer film on titanium bipolar plate for PEMFC, 31382, Copyright 2021, with permission from Elsevier; (d1) SEM image revealing the cross-section of CrN/TiN-coated 316L SS; (d2) potentiodynamic polarization curves of CrN/TiN-coated 316L SS. Reprinted from *Int. J. Hydrogen Energy*, 46, N. Rojas, M. Sánchez-Molina, G. Sevilla, *et al.*, Coated stainless steels evaluation for bipolar plates in PEM water electrolysis conditions, 25929, Copyright 2021, with permission from Elsevier.

between layers of a multilayer structure. The order in which coatings are arranged determines their internal interaction and the extent of their bond to the metal substrate. Reducing the coating thickness improves the compactness of the assembled PEMWE, which ensures the efficiency of the entire system. Thus, multilayer coatings show promising prospects through the employment of nanostructures. Multi-layer coating design should follow two principles. First, the electrical conductivity of the inner layer, which should closely bond with the substrate, must be ensured. Second, the outer layer should possess a corrosion-resistant and hydrophobic structure. Breakthroughs in multilayer coatings may potentially overlook the type of substrate for bipolar plates. Weighty SS materials can be replaced with low-cost, lightweight alloys, such as magnesium, aluminum, and titanium alloys, which considerably reduces the total weight of PEMWE systems. As shown in Fig. 4(d1), Rojas *et al.* [62] prepared CrN/TiN multilayered coatings with 20 bilayers. They observed that CrN/TiN bilayers promoted a good relationship between corrosion resistance and ICR. Under experimental conditions, the pH of these bilayer samples reached 5.5, which is higher than that of the other experiments provided in Table 1.

3.2.2. Carbon-based coatings

The carbon-based coatings used on bipolar plates are mainly classified into pure carbon films and graphitized coatings [7]. The preparation methods for carbon-based coatings include magnetron sputtering, electrochemical deposition, physical vapor deposition (PVD), and chemical vapor deposition (CVD). Carbon-based coatings have excellent electrical conductivity but comparatively weak corrosion resistance. Pure carbon films are susceptible to damage, which can lead to substantial performance degradation of bipolar plates after a short service period [85]. The nanostructuring treatment can be used to obtain dense and defect-free films, which ensure the stable performance of bipolar plates during long-term service. As revealed in Fig. 5(a1)–(a4), the study of 316L SS with nano-amorphous carbon (a-C) films showed the poorest corrosion resistance in the samples with a carbon-layer thickness of 101 nm [63]. This combination of coating and substrate had the best performance statistics (Table 1). The in-

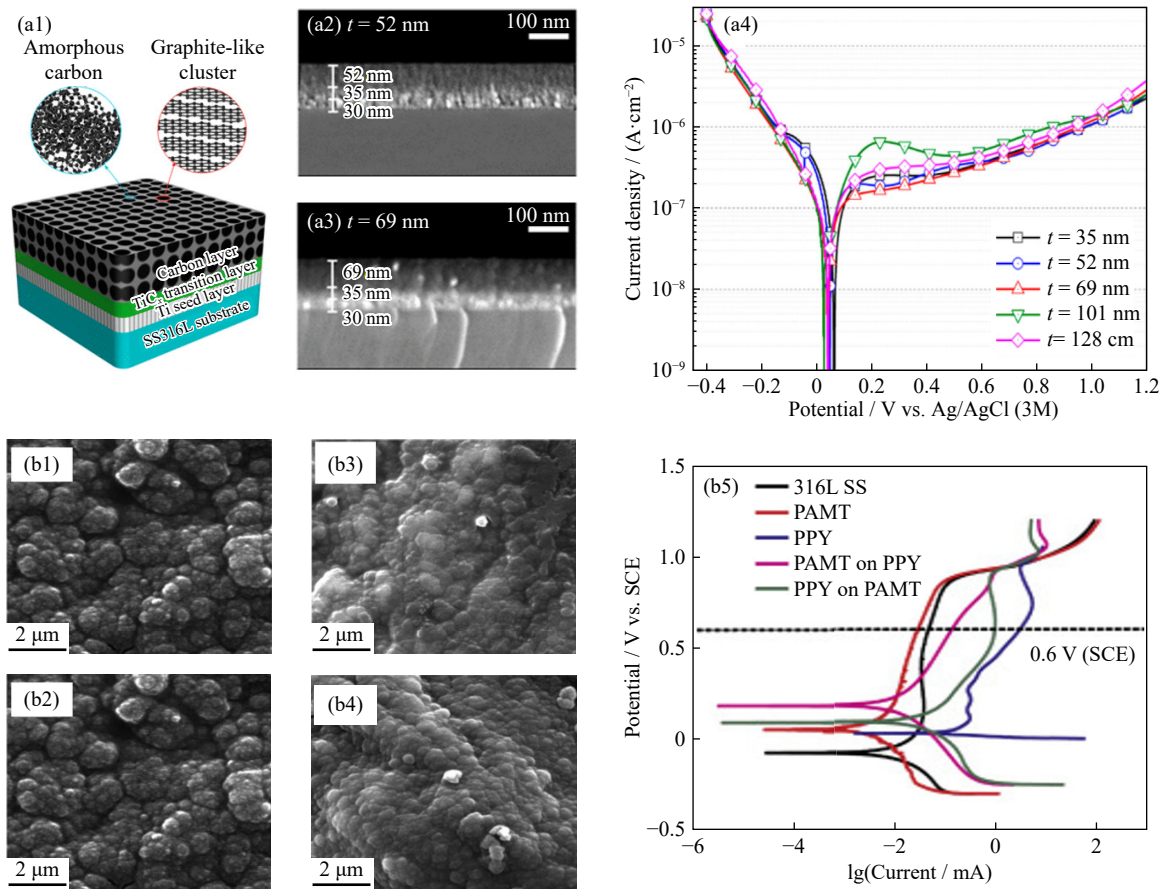

Fig. 5. Analysis of carbon-based and polymer coatings: (a1) preparation of the nanolayered TiC$_x$/a-C film, which included a Ti seed layer, a nanocomposite TiC$_x$ transition layer, and a nanothin a-C film; (a2–a3) SEM image revealing a cross-section of nanothin a-C film with thicknesses (t) of 52 and 69 nm, respectively; (a4) potentiodynamic polarization curves of 316L SS with a nanothin a-C film of different thicknesses. Reprinted with permission from P. Yi, D. Zhang, L. Peng, and X. Lai, *ACS Appl. Mater. Interfaces*, 10, 34561 (2018) [63]. Copyright 2018 American Chemical Society; SEM images of (b1) PPY, (b2) PAMT, (b3) PPY on PAMT, and (b4) PAMT on PPY-coated 316L SS under optimized conditions at different microscopic levels; (b5) potentiodynamic polarization curves in the cathodic environment. Reprinted from *Int. J. Hydrogen Energy*, 46, S. Akula, P. Kalaiselvi, A.K. Sahu, and S. Chellammal, Electrodeposition of conductive PAMT/PPY bilayer composite coatings on 316L stainless steel plate for PEMFC application, 17909, Copyright 2021, with permission from Elsevier.

creased thickness of the a-C layer results in stress relaxation, and vacancy-like defects increase in abundance. Corrosion of the amorphous transition layer in thin a-C layers may result in increased corrosion current density. The carbon nanofilms prepared via sputtering prevent stress relaxation and vacancy loss. In addition, intercalated graphite nanoclusters create a localized protocell effect with amorphous carbon components, which provides protection against corrosion damage [86]. Doping treatment can effectively improve the corrosion resistance of composite carbon films. The enhanced conductivity observed in a-C films can be attributed to the elevated proportion of C sp^2 orbitals [87].

3.2.3. Polymer coatings

Conductive polymers can possess a combination of electrical conductivity and corrosion resistance. Conductive polymer coatings applied to bipolar plates are mainly categorized as polyaniline (PANI) [88–89] and polypyrrole (PPY) [64,90] films. A study on PPY and PAMT coatings (Fig. 5(b1)–(b5)) revealed that the double-layer coatings were better than the single-layer ones. This type of coating delayed the onset of corrosion by lengthening the diffusion path of the corrosive medium between the metal and coatings. Copper plates coated with a double-layer polypyridine/PANI composite film showed a more negative corrosion potential than those with single-layer polypyridine films. The composite films improved the corrosion resistance by blocking the entry of some ions. However, the specimens coated with composite film had a large ICR [91]. Doping with organic or inorganic substances increases the structural stability of conducting polymers. The doped inorganic materials generally include carbon [91] and titanium oxides [92] due to their desirable electrical conductivity and corrosion resistance. Doped nanoparticles are used to improve the densification of polymer films [93], and doping with noble metals increases electrical conductivity [94]. Conductive polymers are qualified candidates, given their simple and inexpensive manufacturing procedure. However, polymer coatings are prone to porosity and do not guarantee performance stability under the operating conditions of PEMWEs. Problems related to these coating requirements can be addressed through endeavors on several aspects, including the improvement of electrical conductivity, performance stability in long-term operation, and adhesion between coatings and substrates. Currently, studies are focusing on the modification of polymer coatings, mainly through doping of different kinds of inorganic conductive particles. The formation of inorganic–organic compounds with strong bonding strength will further advance the application of polymer coatings.

4. Structural design

PEMWEs have a fluid-flow condition that is more similar to that in direct methanol fuel cells (DMFC) than that in PEMFCs [95]. PEMWEs and DMFCs contain higher proportions of liquid-phase substances than gas-phase substances. As a reactant, pure water offers lower cost and higher safety compared with hydrogen. Therefore, PEMWEs can ensure efficiency by increasing water flow, while PEMFCs will not increase hydrogen flow for safety and cost reasons. The stoichiometric ratio (ξ) refers to the ratio of reactant supply to reactant consumption. The ξ for pure water in PEMWEs can be above 50 [96–97], and that for hydrogen and oxygen in PEMFCs usually does not exceed 4 [98–99]. The research on hydrogen and oxygen as PEMFCs' reactants needs to focus on safety and economy. Thus, the ξ should not be extremely high. For PEMWEs, the principal objective of flow-field design focuses on ensuring stable operations through meticulous consideration of pressure and heat distributions. The ξ of reactants can be increased directly to optimize the reactant supply on the surface of the catalytic layer. In PEMWEs, the diffusion resistance of the electrochemical reaction is minimized as much as possible, and the electron transfer resistance serves as a rate-controlling step. PEMWE development will further move toward attaining high pressure and high potential (Section 2). In this case, the appropriate flow-field design with uniform flow and pressure distribution developed into a research challenge. In the flow-field design session, iterative optimization is usually performed using macroscopic model simulation [100–101]. The volume-of-fluid method simulations at low potentials usually yield highly accurate cloud distributions of pressure and temperature in the flow channel, and the simulation results at high potentials deviate considerably from experimental findings. Wu *et al*. [96,102] improved the accuracy of simulation results at high potentials through mesoscopic–macroscopic and experimental–macroscopic coupling simulation.

4.1. Channel-rib flow field

The design of channel-rib structures, which offer a service life of over 20 years, is more traditional compared with those of other structures [103–104]. The channel portion serves as a transmission medium for liquids and gases, and the rib portion conducts electricity and heat. In laboratory settings, the area of bipolar plates is limited to a certain extent. By contrast, automotive PEMFCs and commercial PEMWEs feature bipolar plates with substantially large areas.

The large area release facilitates various and complex flow-field designs, such as the multichannel serpentine flow field in Fig. 6(a) [105]. Diversified channel-rib flow fields can be used to mimic biological structures [106]. As shown in Fig. 6(b), the width scaling parameters with tree-like patterns in the bipolar plates used in PEMFCs reduced viscous dissipation in the channels [107]. The use of a lung-like flow design resulted in uniform reactant distribution across the electrodes and a minimal entropy generated by the entire system (Fig. 6(c)) [108]. The improvement of the convective effect of the reactant fluid from the flow field to the catalytic layer mitigates the concentration loss in the electrochemical reaction. Baffles in flow channels promote convection; they have the advantage of increasing the supply of reactants and the disadvantage of increased pumping power. As PEMWEs and PEMFCs are considered small reactors, the enhance-

ment degree evidently corresponds to the baffle shape. Ghanbarian *et al.* [109] considered the effect of the addition of square, semicircular, and trapezoidal baffles on the power of PEMFCs. Yin *et al.* [110] investigated the front and rear bottom angles of a trapezoidal baffle and observed that the reactant transport performance and system output power were optimal when the front and rear bottom angles were 45° (Fig. 6(d)). A channel with a best-in-class trapezoidal baffle increased the current density by 17.7% compared with a non-baffled channel. Another option is to optimize the shape of vertical walls associated with the gas diffusion layer (GDL) on both sides of the flow channel. A new droplet flow-field structure proposed by Meng *et al.* [49] increased the maximum power density by 23.7% compared with the parallel flow field (Fig. 6(e)). Wang *et al.* [111] implemented a tapered flow-field configuration to achieve the uniform distribution of reactants and current density. The coefficients of variation for the current density and oxygen molar concentration were reduced by approximately 21.4% and 8.5%, respectively. The findings of Xu *et al.* [112] on the structure of wave-shaped flow channels revealed that mass transfer by gas diffusion can be improved by introducing a groove structure in the GDL. In addition, adjustment of the width or depth of channels and ribs can improve pressure distribution and system power. However, all of the above methods have side effects, such as increased pump power and difficulty in drainage.

The areas for gas/liquid transfer and current/heat conduction are mathematically equivalent based on the same width value of channels and ribs [109–110]. Metallic bipolar plates are usually highly conductive, and thus, ohmic losses for

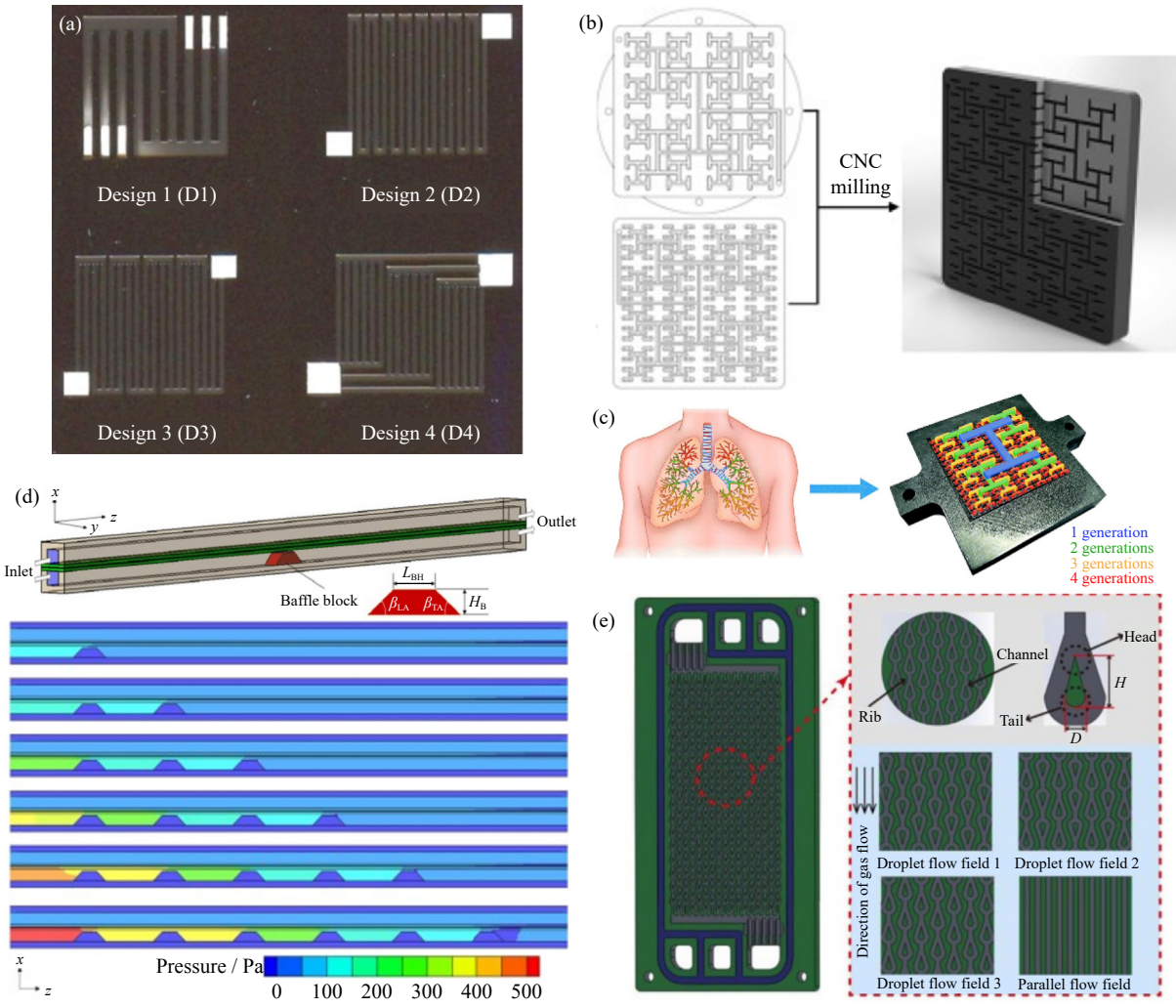

Fig. 6. Optimized design study based on channel-rib flow-field structure: (a) optimization of arrangement based on traditional parallel and serpentine flow channels. Reprinted from *J. Power Sources*, 195, Y.H. Lu and R.G. Reddy, Performance of micro-PEM fuel cells with different flow fields, 503, Copyright 2010, with permission from Elsevier; (b) tree-like flow-field design based on biomimetic concepts [107]; (c) lung-like flow-field design based on biomimetic concepts [108]; (d) flow-field design with baffle plates added to the channel for the improved mass transfer. Reprinted from *Appl. Energy*, 271, Y. Yin, S.Y. Wu, Y.Z. Qin, O.N. Otoo, and J.F. Zhang, Quantitative analysis of trapezoid baffle block sloping angles on oxygen transport and performance of proton exchange membrane fuel cell, 11527, Copyright 2020, with permission from Elsevier; (e) droplet-shaped flow design obtained by changing the curvature of sidewalls of the flow channel Reprinted from *Chem. Eng. J.*, 450, X.C. Meng, H. Ren, J.K. Hao, and Z.G. Shao, Design and experimental research of a novel droplet flow field in proton exchange membrane fuel cell, 138276, Copyright 2022, with permission from Elsevier.

their electrochemical reactions are relatively negligible. Appropriate reduction of conductive interfaces and the increase in mass transfer interfaces can considerably optimize gas and liquid transport processes without substantially increasing ohmic losses [113].

4.2. Porous flow field

High-porosity porous materials are expected to replace conventional flow fields. Representative porous materials in some PEMFCs include metal foams, sintered minerals, porous plates, and 3D meshes [114–115]. The increase in porosity improves the contact area between channels and the GDL, which results in the optimized transport process of gases and liquids. The porosity value of porous materials with uniformly distributed pores is equivalent to the ratio of the contact area between the ribs and GDL to the total area of bipolar plates in the channel-rib flow field. Electronic conduction results in negligible ohmic losses due to the small pore size of the porous structure, which causes the narrowing of the electronic conduction path [116]. Porous structures not only become more uniform in stress distribution under extrusion but are also lighter in weight than channel-rib structures.

Various commercial examples of porous structured flow fields have now become accessible. As shown in Fig. 7(a), a 3D fine-grid porous flow field designed for the Mirai fuel-cell vehicle produced by Toyota Company remarkably enhanced the transport process of reactants to the catalytic layer [117]. As shown in Fig. 7(b), the NEXO fuel cell of Hyundai Company incorporates a novel porous plate design aimed at minimizing concentration losses during the reaction through innovative technology production [114].

The porous-structure flow field shows a greater potential compared with the conventional channel-rib flow field. To advance the application of porous flow fields, scholars should focus more on fabrication methods, characterization techniques, and structural design. Furthermore, efforts to diminish costs are supposed to be achieved using the power of the system guaranteed in the meantime in the porous flow field.

4.3. Innovative structure

The innovative additive manufacturing technology, also known as 3D printing, constructs objects through the addition and stacking of materials layer by layer [118–119]. Additive manufacturing can be used to create complex geometric structures, such as internal cavities, curves, and skeletonized structures. Manufacturing goals achieved through this method are accomplished without complex processes and numerous tools compared with traditional manufacturing techniques. In addition, metal additive manufacturing minimizes material waste by using recycled powders during printing. The high resource utilization of additive manufacturing matches the low-carbon and environmentally friendly concept of hydrogen economy. In summary, additive manufacturing technology is promising for PEMFC and PEMWE flow-field plate manufacturing. Stable outputs of PEMWEs and PEMFCs can be achieved through the interruption of air bubble buildup via a dual-layer channel design. As displayed in Fig. 8(a), Xu *et al.* [120] reported that the PEMWE with a double-layer channel flow field was improved by 0.171 V at 3 A·cm^{-2} compared with the conventional parallel flow field. With the use of the new dual-layer channel flow field, the distribution of temperature and current density becomes more uniform, which has a positive influence on the durability and performance of PEMWEs. As shown in Fig. 8(b), Chen *et al.* [121] designed a novel two-layer channel flow field via 3D printing to improve oxygen concentration and drainage performance under the rib. They solved the trilemma related to the performance, pressure drop, and manufacturing feasibility.

As shown in Fig. 8(c), Yang *et al.* [59,122–124] explored the feasibility of 3D printing technology for PEMWE applic-

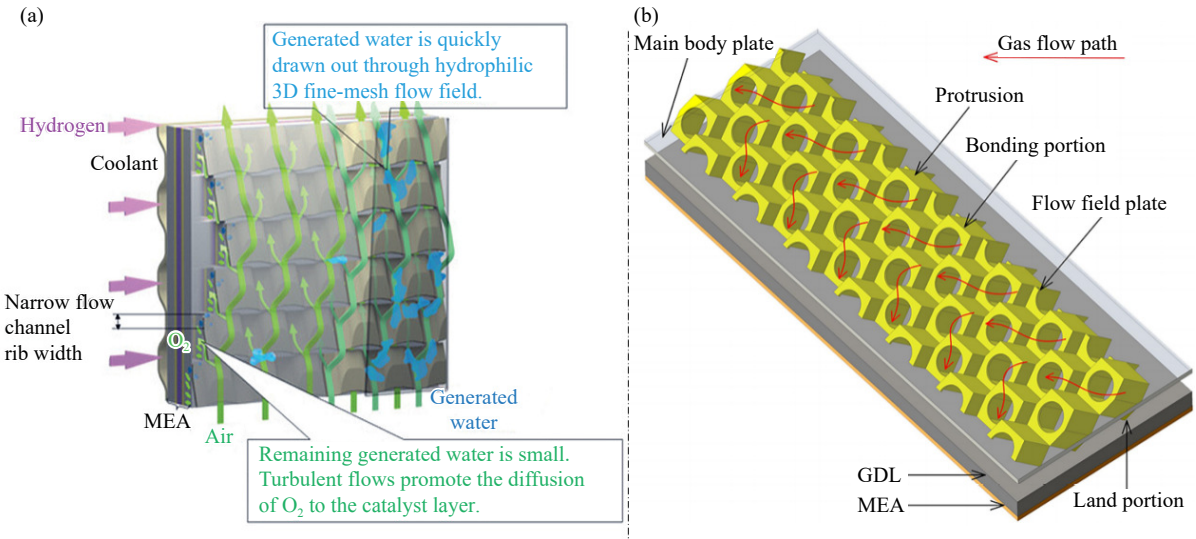

Fig. 7. Current representative porous flow-field bipolar plates: (a) a three-dimensional fine-grid porous flow field designed for Mirai fuel-cell vehicle produced by Toyota. Y. Wang, D.F. Ruiz Diaz, K.S. Chen, Z. Wang, and X.C. Adroher, *Mater. Today*, 32, 178 (2020) [117]. Copyright Wiley-VCH Verlag GmbH & Co. KGaA. Reproduced with permission; (b) a new type of porous plate in NEXO fuel-cell manufactured by Hyundai. Reprinted with permission from G. Zhang, Z. Qu, W.Q. Tao, *et al.*, *Chem. Rev.*, 123, 989 (2023) [114]. Copyright 2018 American Chemical Society.

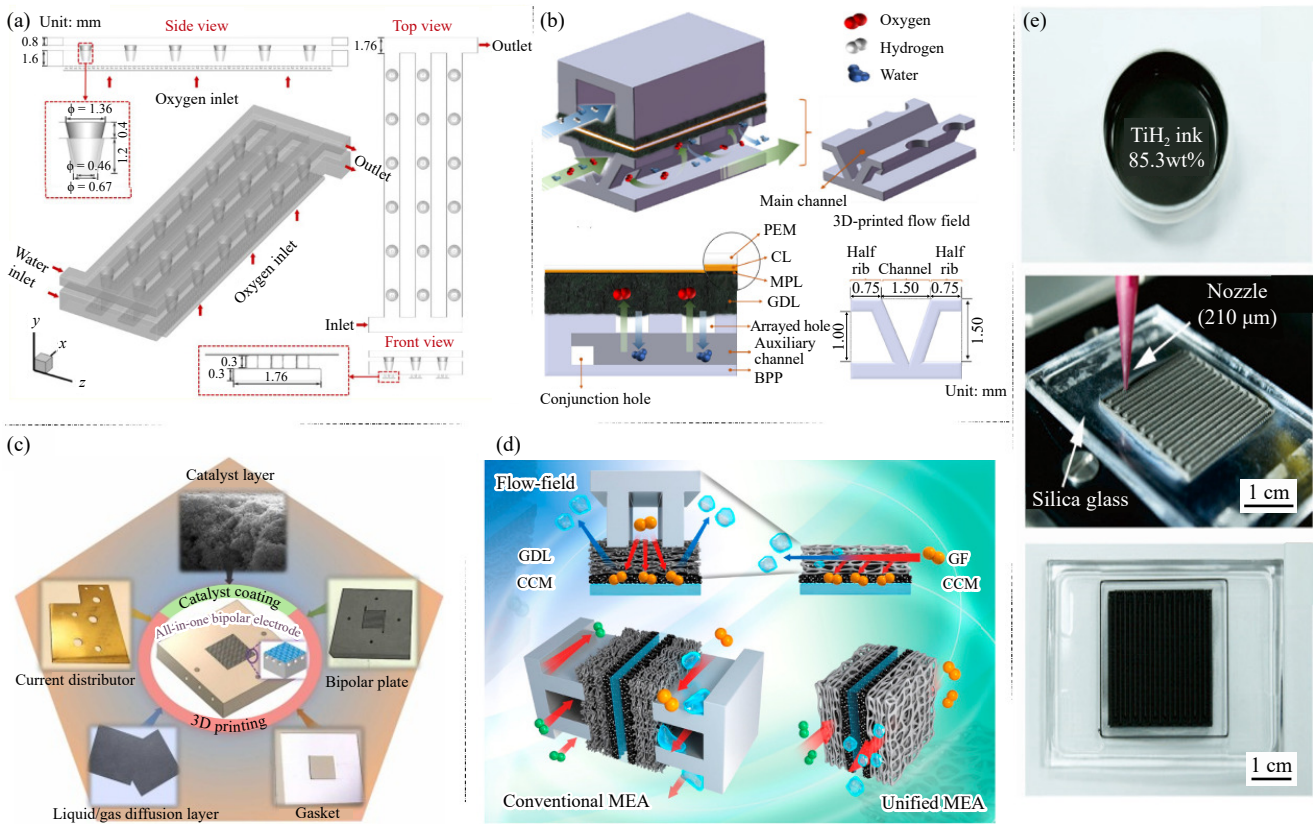

Fig. 8. Several novel and recently introduced flow-field structure designs: (a) double-layer structure proposed to solve the problem of parallel flow field with oxygen bubbles aggregated on the diagonal sider. Reprinted from *Digit. Chem. Eng.*, 1, Y.F. Xu, G.B. Zhang, L.Z. Wu, Z.M. Bao, B.F. Zu, and K. Jiao, A 3-D multiphase model of proton exchange membrane electrolyzer based on open-source CFD, 100004, Copyright 2021, with permission from Elsevier; (b) novel flow field obtained via 3D printing of auxiliary channels with transplanter aligned holes. G.J. Chen, W.D. Shi, J. Xuan, *et al.*, *AIChE. J.*, 68, e17758 (2022) [121]. Copyright Wiley-VCH Verlag GmbH & Co. KGaA. Reproduced with permission; (c) all-in-one bipolar electrode with an integrated catalyst layer, a GDL, a flow field plate, a current divider, and a spacer. Reprinted from *Nano Energy*, 90, G.Q. Yang, Z.Q. Xie, S.L. Yu, *et al.*, All-in-one bipolar electrode: A new concept for compact and efficient water electrolyzers, 106551, Copyright 2021, with permission from Elsevier; (d) graphene foam acting as a flow field and a GDL. Reprinted from *Electrochim. Acta*, 323, J.E. Park, J. Lim, M.S. Lim, *et al.*, Gas diffusion layer/flow-field unified membrane-electrode assembly in fuel cell using graphene foam, 134808, Copyright 2019, with permission from Elsevier; (e) novel design of flow field–gas diffusion layers generated by 3D printing of TiH_2 and pyrolysis. Reprinted from *J. Power Sources*, 515, X.C. Wang, H.L. Ma, H.Q. Peng, *et al.*, Enhanced mass transport and water management of polymer electrolyte fuel cells via 3-D printed architectures, 230636, Copyright 2021, with permission from Elsevier.

ations for the innovative design and fabrication of an all-in-one flow structure. Their work was the first to integrate a liquid/GDL, a bipolar plate, a spacer, and a current distributor into a single multifunctional plate without using tools or molds. Recent research indicated the impressive energy efficiency of the electrolyzer (86.48%) at 2 $A \cdot cm^{-2}$ and 80°C. The energy efficiency surpassed that of conventional electrolyzers by 61.81% in terms of hydrogen production rate.

Integrated structural design is also a way forward to enhance the performance of PEMWEs and PEMFCs. In Fig. 8(d), Park *et al.* [125] replaced the existing flow field and GDL with 3D graphene foam. Despite its low mechanical strength, the 3D graphene foam ensured corrosion resistance and hydrophobicity without a coating treatment. Electron conduction paths and reactant transport were notably reduced through the integration of a gas diffusion layer and a flow-field, which decreased ohmic losses during electrochemical reactions. The structure designed by Wang *et al.* [126] integrates a flow field plate with a GDL to obtain unique and regular gas flow channels via 3D printing (Fig. 8(e)). In addition, the integrated structure saves space by minimizing the battery thickness. In the design of an integrated flow field using porous materials, a large ICR may arise due to the considerable difference in pore size between the catalytic layer and porous material [127]. An integrated flow field with a gradient distribution of pore sizes was designed to ameliorate this problem, but it increased the cost of fabrication.

5. Interaction of material selection and structural design

In the design process of bipolar plates, typically there is a focus on their corrosion behavior under high potential and oxygen/hydrogen-rich and acidic conditions. The design of the flow-field structure prioritizes the uniform distribution of water and heat. With the aim of promoting the synergistic design of bipolar plates, mutual concerns are summarized

elaborately, with various considerations taken into account in the following section.

5.1. Influence of material selection on mass and heat transfer

Types of materials consider the electrical and thermal conductivity properties. Electrical conductivity governs heat generation, and thermal conductivity determines heat dissipation capability. As a result of poor electrical conductivity, ohmic voltage drops, electrical losses increase, and unstable system operation transpires due to excessive heat generation in the pole plate. A single metal bipolar plate exhibits excellent electrical and thermal conductivity. However, heat accumulation occurs when multiple bipolar plates are stacked due to ICR. In addition, a high material thermal capacity leads to a stable heat transfer process. As an effective method of reducing temperature, the addition of coolant has become the mainstream choice of engineering cooling [128].

The hydrophobic nature of the coating applied on bipolar plates plays an important role in controlling gas and liquid flow. In parameter measurement, the contact angle of a droplet can illustrate hydrophobicity. A high level of hydrophobicity in the coating for water electrolyzers and fuel cells is conducive to system efficiency via an improved mass transfer [129]. The efficiency of mass transfer in porous flow fields is directly influenced by the permeability of the selected material. Materials with a high permeability can facilitate the mass transfer process through the formation of a generous path for ions to divert through their surface or micropores [130].

A material's corrosion resistance, high-temperature resistance, and mechanical strength influence the service life and stability of bipolar plates. Elaborate selection of materials ensures the durability of bipolar plates against corrosion, rupture, and deformation during long-term use, providing a stable mass and heat transfer performance.

Corners impede heat and mass transfer processes, although they represent a small percentage of the total flow channel in conventional parallel and serpentine flow fields. A possible approach is covering corners with hydrophobic coatings to reduce fluid resistance. This method improves the overall mass and heat transfer performance of bipolar plates through the sacrifice of local electrical conductivity. Furthermore, given the differences in gas-to-liquid ratio at the inlet and outlet of the flow field, some researchers have adopted gradient-designed flow-field structures in the further optimization of the performance of bipolar plates. Similarly, the surface properties of bipolar plates can be modified through the gradient design of the composition and structure of coating materials. In the future, each channel within the same flow field may exhibit distinct hydrophobicity and electrical conductivity levels. This innovative approach holds the potential for substantial improvement of the comprehensive performance of the PEMFC and PEMWE systems.

5.2. Influence of structural design on corrosion

Structural design is mainly aimed at maximizing power output. If the material performance is notably better than the engineering requirements, investing considerable amounts of money in structural design is unnecessary. However, expectations of the power output from water electrolysis and fuel cells have increased with the performance of new materials. New manufacturing processes and materials benefit the realization of more complex structural designs.

A properly engineered flow-field structure aims to mitigate corrosion risk, enhance service longevity, and bolster stability by optimizing media distribution and managing velocity and pressure through effective buffering and dispersal functions. Accelerate material depletion may result from excessive velocities and high pressures. Excessive pressure and temperature damage to the system is avoided via the setting of buffer zones, which will equalize the pressure and temperature of the entire system. Dispersion zones uniformly disperse reactants over an entire electrode surface to improve the efficiency and homogeneity of the reaction. The medium was adequately diffused and dispersed through the increased number of inlet channels [131]. The PEMWE system is currently being developed toward larger sizes, and higher flow velocities will be obtained in the flow field in the future. Corrosion on bipolar plates will occur to a greater extent in turbulent conditions, considering a wider contact range of oxygen or other corrosive substances in the fluid.

The flow is typically fast, and the temperature is high at the bending sections and the top of baffles in PEMWEs. The oxygen concentration gradually increases with a decrease in the distance from the outlet. Flow disturbances and improved curvature prevent localized accumulation of corrosive media. Maintaining a uniform distribution of the medium contributes to the prolonged lifespan of bipolar plates. In this regard, porous flow fields are preferable over traditional ribbed flow fields.

6. Conclusions and prospects

In this review, we present the current state of material selection and structural design in the design of PEMWE bipolar plates. Differences in the performances required for bipolar plates of PEMFCs and PEMWEs are mainly attributed to their operating conditions, which render material with superior properties suggested for PEMWEs than the former. The proper selection of materials not only improves corrosion resistance but also ensures stable heat and mass transfer processes. An excellent structural design can prolong the service life of bipolar plates and reduce the diffusion resistance of electrochemical reactions. Fig. 9 depicts the current status of material selection and structure design.

New operating conditions require the use of high-performance bipolar plates. In the future, PEMWEs will be run at high currents to increase the hydrogen production capacity. Coatings are particularly susceptible to failure at high potentials. The dissolution of coatings will result in substrate exposure and catalyst layer poisoning. All of these have a negative effect on the service life of PEMWEs. At high potentials, PEMWEs accelerate the supply of reactants, which ex-

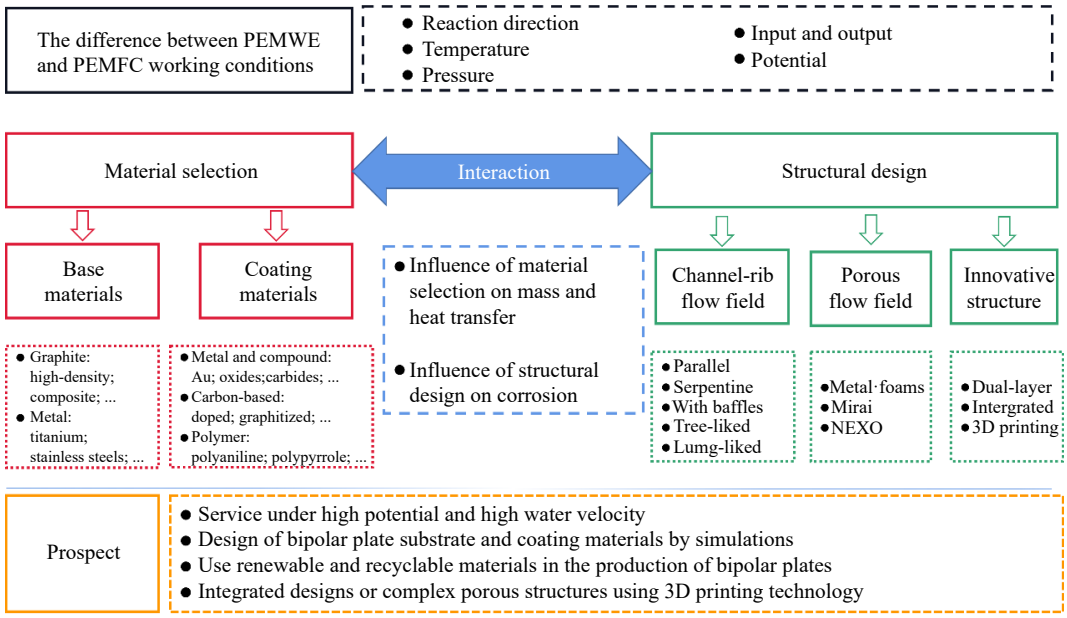

Fig. 9. Illustration of overview and prospects on bipolar plates.

acerbates the damage on the surface of bipolar plates due to the simultaneous increase in flow rate and oxygen content. In addition, the trend toward larger PEMWEs places new demands on the manufacturing process of bipolar plates. Large bipolar plates require additional improvements in runner molding accuracy and a uniform addition of surface coatings.

New design concepts can open up opportunities for bipolar plates. The introduction of computer and simulation technology is expected to increase the efficiency and accuracy of material innovation through optimization of their composition and organization compared with the traditional method that uses experimental trial and error. The corrosion resistance and electrical conductivity of new materials can be explained at the microscopic scale by simulations, such as first-principles calculations, molecular dynamics, and phase fields. Through calculation, the Gibbs free energy that reflects the exchange current density of the corrosion reaction on bipolar plates can be obtained. The electronic structure considered in the calculation results can be indicative of a material's conductivity. If renewable and recyclable materials can be used to manufacture bipolar plates, an environmentally friendly hydrogen production system becomes accessible.

The application of new manufacturing technologies will raise the upper limit of bipolar-plate performance. Computer simulations can be used in the design of flow-field structures, and 3D printing can be applied in the rapid fabrication of complex simulated designs in a relatively short period. Meanwhile, 3D printing for direct manufacture can be conducted without considering processes and tools, which reduces the development cycle time. This technology can be used to construct porous flow fields with complex pore structures to ensure stable heat and mass transfer in PEMWEs. Finally, the decrease in ICR and lightweight design can be obtained simultaneously through the integrated design based on 3D printing technology.

Acknowledgements

This work was supported by the National Natural Science Foundation of China (No. 52125102), the National Key Research and Development Program of China (No. 2021YFB4000101), and Fundamental Research Funds for the Central Universities (No. FRF-TP-2021-02C2).

Conflict of Interest

Chaofang Dong is an editorial board member for this journal and was not involved in the editorial review or the decision to publish this article. The authors declare that they do not have any competing financial interests or personal relationships that could have appeared to influence the work reported in this paper.

References

[1] I. Staffell, D. Scamman, A. V. Abad, *et al*., The role of hydrogen and fuel cells in the global energy system, *Energy Environ. Sci.*, 12(2019), No. 2, p. 463.

[2] M.L. Yue, H. Lambert, E. Pahon, R. Roche, S. Jemei, and D. Hissel, Hydrogen energy systems: A critical review of technologies, applications, trends and challenges, *Renewable Sustainable Energy Rev.*, 146(2021), art. No. 111180.

[3] R.W. Howarth and M.Z. Jacobson, How green is blue hydrogen?, *Energy Sci. Eng.*, 9(2021), No. 10, p. 1676.

[4] X. Liu, G.Y. Liu, J.L. Xue, X.D. Wang, and Q.F. Li, Hydrogen as a carrier of renewable energies toward carbon neutrality: State-of-the-art and challenging issues, *Int. J. Miner. Metall. Mater.*, 29(2022), No. 5, p. 1073.

[5] S.A. Grigoriev, V.N. Fateev, D.G. Bessarabov, and P. Millet, Current status, research trends, and challenges in water electrolysis science and technology, *Int. J. Hydrogen Energy*, 45(2020), No. 49, p. 26036.

[6] M. David, C. Ocampo-Martínez, and R. Sánchez-Peña, Advances in alkaline water electrolyzers: A review, *J. Energy Storage*, 23(2019), p. 392.

[7] X.J. Luo, C.H. Ren, J. Song, *et al*., Design and fabrication of bipolar plates for PEM water electrolyser, *J. Mater. Sci. Technol.*, 146(2023), p. 19.
[8] Z.Y. Kang, T. Schuler, Y.Y. Chen, M. Wang, F.Y. Zhang, and G. Bender, Effects of interfacial contact under different operating conditions in proton exchange membrane water electrolysis, *Electrochim. Acta*, 429(2022), art. No. 140942.
[9] S. Lædre, C.M. Craciunescu, T. Khoza, *et al*., Issues regarding bipolar plate-gas diffusion layer interfacial contact resistance determination, *J. Power Sources*, 530(2022), art. No. 231275.
[10] X.J. Luo, L.Q. Chang, C.H. Ren, *et al*., Sandwich-like functional design of C/(Ti:C)/Ti modified Ti bipolar plates for proton exchange membrane fuel cells, *J. Power Sources*, 585(2023), art. No. 233633.
[11] X.Z. Yuan, C. Nayoze-Coynel, N.M. Shaigan, *et al*., A review of functions, attributes, properties and measurements for the quality control of proton exchange membrane fuel cell components, *J. Power Sources*, 491(2021), art. No. 229540.
[12] M. Hala, J. Mališ, M. Paidar, and K. Bouzek, Characterization of commercial polymer-carbon composite bipolar plates used in PEM fuel cells, *Membranes*, 12(2022), No. 11, art. No. 1050.
[13] N.A. Mohd Radzuan, A.B. Sulong, and M.R. Somalu, Influence the filler orientation on the performance of bipolar plate, *Sains Malays.*, 48(2019), No. 3, p. 669.
[14] H.X. Cheng, H. Luo, X.F. Wang, *et al*., Improving the performance of titanium bipolar plate in proton exchange membrane water electrolysis environment by nitrogen–chromium composite cathode plasma electrolytic deposition, *Int. J. Hydrogen Energy*, 48(2023), No. 98, p. 38557.
[15] B. Xie, G.B. Zhang, Y. Jiang, *et al*., "3D+1D" modeling approach toward large-scale PEM fuel cell simulation and partitioned optimization study on flow field, *eTransportation*, 6(2020), art. No. 100090.
[16] W.T. Pan, P.H. Wang, X.L. Chen, F.C. Wang, and G.C. Dai, Combined effects of flow channel configuration and operating conditions on PEM fuel cell performance, *Energy Convers. Manage.*, 220(2020), art. No. 113046.
[17] E. Rahmani, T. Moradi, S. Ghandehariun, G.F. Naterer, and A. Ranjbar, Enhanced mass transfer and water discharge in a proton exchange membrane fuel cell with a raccoon channel flow field, *Energy*, 264(2023), art. No. 126115.
[18] W. Gao, Q.F. Li, K. Sun, R. Chen, Z.Z. Che, and T.Y. Wang, Mass transfer and water management in proton exchange membrane fuel cells with a composite foam-rib flow field, *Int. J. Heat Mass Transf.*, 216(2023), art. No. 124595.
[19] T.J. Pan, Y.J. Dai, J. Jiang, J.H. Xiang, Q.Q. Yang, and Y.S. Li, Anti-corrosion performance of the conductive bilayer CrC/CrN coated 304SS bipolar plate in acidic environment, *Corros. Sci.*, 206(2022), art. No. 110495.
[20] A. Kellenberger, D. Duca, N. Vaszilcsin, and C.M. Craciunescu, Electrochemical evaluation of niobium corrosion resistance in simulated anodic PEM electrolyzer environment, *Int. J. Electrochem. Sci.*, 15(2020), No. 11, p. 10664.
[21] J. Jin, J.Z. Zhang, M.L. Hu, and X. Li, Investigation of high potential corrosion protection with titanium carbonitride coating on 316L stainless steel bipolar plates, *Corros. Sci.*, 191(2021), art. No. 109757.
[22] S. Simaafrookhteh, M. Khorshidian, and M. Momenifar, Fabrication of multi-filler thermoset-based composite bipolar plates for PEMFCs applications: Molding defects and properties characterizations, *Int. J. Hydrogen Energy*, 45(2020), No. 27, p. 14119.
[23] F. Roncaglia, M. Romagnoli, S. Incudini, *et al*., Graphite-epoxy composites for fuel-cell bipolar plates: Wet vs dry mixing and role of the design of experiment in the optimization of molding parameters, *Int. J. Hydrogen Energy*, 46(2021), No. 5, p. 4407.
[24] J. Chen, R.L. Fan, Y.H. Peng, *et al*., Tuning the performance of composite bipolar plate for proton exchange membrane fuel cell by modulating resin network structure, *J. Power Sources*, 582(2023), art. No. 233566.
[25] L.X. Fan, Y. Liu, X.B. Luo, Z.K. Tu, and S.H. Chan, A novel gas supply configuration for hydrogen utilization improvement in a multi-stack air-cooling PEMFC system with dead-ended anode, *Energy*, 282(2023), art. No. 129004.
[26] J. Shen, L.P. Zeng, Z.C. Liu, and W. Liu, Performance investigation of PEMFC with rectangle blockages in Gas Channel based on field synergy principle, *Heat Mass Transf.*, 55(2019), No. 3, p. 811.
[27] J.C. Kurnia, A.P. Sasmito, and T. Shamim, Advances in proton exchange membrane fuel cell with dead-end anode operation: A review, *Appl. Energy*, 252(2019), art. No. 113416.
[28] Q. Feng, X.Z. Yuan, G.Y. Liu, *et al*., A review of proton exchange membrane water electrolysis on degradation mechanisms and mitigation strategies, *J. Power Sources*, 366(2017), p. 33.
[29] G. Bender, M. Carmo, T. Smolinka, *et al*., Initial approaches in benchmarking and round robin testing for proton exchange membrane water electrolyzers, *Int. J. Hydrogen Energy*, 44(2019), No. 18, p. 9174.
[30] E. Kuhnert, M. Heidinger, D. Sandu, V. Hacker, and M. Bodner, Analysis of PEM water electrolyzer failure due to induced hydrogen crossover in catalyst-coated PFSA membranes, *Membranes*, 13(2023), No. 3, art. No. 348.
[31] E. Chalkova, M.V. Fedkin, S. Komarneni, and S.N. Lvov, Nafion/zirconium phosphate composite membranes for PEMFC operating at up to 120°C and down to 13% RH, *J. Electrochem. Soc.*, 154(2007), No. 2, art. No. B288.
[32] S. Ryu, B. Lee, J.H. Kim, C. Pak, and S.H. Moon, High-temperature operation of PEMFC using pore-filling PTFE/Nafion composite membrane treated with electric field, *Int. J. Energy Res.*, 45(2021), No. 13, p. 19136.
[33] A. Lotrič, M. Sekavčnik, I. Kuštrin, and M. Mori, Life-cycle assessment of hydrogen technologies with the focus on EU critical raw materials and end-of-life strategies, *Int. J. Hydrogen Energy*, 46(2021), No. 16, p. 10143.
[34] W. Xu, K. Scott, and S. Basu, Performance of a high temperature polymer electrolyte membrane water electrolyser, *J. Power Sources*, 196(2011), No. 21, p. 8918.
[35] I. Dedigama, K. Ayers, P.R. Shearing, and D.J.L. Brett, An experimentally validated steady state polymer electrolyte membrane water electrolyser model, *Int. J. Electrochem. Sci.*, 9(2014), No. 5, p. 2662.
[36] V.K. Puthiyapura, M. Mamlouk, S. Pasupathi, B.G. Pollet, and K. Scott, Physical and electrochemical evaluation of ATO supported IrO_2 catalyst for proton exchange membrane water electrolyser, *J. Power Sources*, 269(2014), p. 451.
[37] H.C. Chen, Z. Liu, X.C. Ye, L. Yi, S.C. Xu, and T. Zhang, Air flow and pressure optimization for air supply in proton exchange membrane fuel cell system, *Energy*, 238(2022), art. No. 121949.
[38] V. Lakshminarayanan and P. Karthikeyan, Performance enhancement of interdigitated flow channel of PEMFC by scaling up study, *Energy Sources Part A*, 42(2020), No. 14, p. 1785.
[39] C. Werner, L. Busemeyer, and J. Kallo, The impact of operating parameters and system architecture on the water management of a multifunctional PEMFC system, *Int. J. Hydrogen Energy*, 40(2015), No. 35, p. 11595.
[40] Y.J. Ding, L.F. Xu, W.B. Zheng, *et al*., Characterizing the two-phase flow effect in gas channel of proton exchange membrane fuel cell with dimensionless number, *Int. J. Hydrogen Energy*, 48(2023), No. 13, p. 5250.

[41] X. Zhou, L.Z. Wu, Z.Q. Niu, *et al*., Effects of surface wettability on two-phase flow in the compressed gas diffusion layer microstructures, *Int. J. Heat Mass Transf.*, 151(2020), art. No. 119370.

[42] T. Krenz, O. Weiland, P. Trinke, *et al*., Temperature and performance inhomogeneities in PEM electrolysis stacks with industrial scale cells, *J. Electrochem. Soc.*, 170(2023), No. 4, art. No. 044508.

[43] T. Miličić, H. Altaf, N. Vorhauer-Huget, L.A. Živković, E. Tsotsas, and T. Vidaković-Koch, Modeling and analysis of mass transport losses of proton exchange membrane water electrolyzer, *Processes*, 10(2022), No. 11, art. No. 2417.

[44] M. Fang, J.X. Zou, C. Yin, and Y.T. Song, Prediction and parametric analysis of bubble humidifier performance in a polymer electrolyte membrane fuel cell test system by response surface methodology, *Energy Sources Part A*, 44(2022), No. 2, p. 3497.

[45] M. Li, K.J. Duan, N. Djilali, and P.C. Sui, Flow sharing and turbulence phenomena in proton exchange membrane fuel cell stack headers, *Int. J. Hydrogen Energy*, 44(2019), No. 57, p. 30306.

[46] Y.J. Deng, B. Chi, J. Li, *et al*., Atomic Fe-doped MOF-derived carbon polyhedrons with high active-center density and ultra-high performance toward PEM fuel cells, *Adv. Energy Mater.*, 9(2019), No. 13, art. No. 1802856.

[47] M. Qiao, Y. Wang, Q. Wang, *et al*., Hierarchically ordered porous carbon with atomically dispersed FeN_4 for ultraefficient oxygen reduction reaction in proton-exchange membrane fuel cells, *Angew. Chem. Int. Ed.*, 59(2020), No. 7, p. 2688.

[48] Y.Y. Zhou, Z.Y. Xie, J.X. Jiang, *et al*., Lattice-confined Ru clusters with high CO tolerance and activity for the hydrogen oxidation reaction, *Nat. Catal.*, 3(2020), p. 454.

[49] X.C. Meng, H. Ren, J.K. Hao, and Z.G. Shao, Design and experimental research of a novel droplet flow field in proton exchange membrane fuel cell, *Chem. Eng. J.*, 450(2022), art. No. 138276.

[50] H. Teuku, I. Alshami, J. Goh, M.S. Masdar, and K.S. Loh, Review on bipolar plates for low-temperature polymer electrolyte membrane water electrolyzer, *Int. J. Energy Res.*, 45(2021), No. 15, p. 20583.

[51] M. Phuangngamphan, M. Okhawilai, S. Hiziroglu, and S. Rimdusit, Development of highly conductive graphite-/graphene-filled polybenzoxazine composites for bipolar plates in fuel cells, *J. Appl. Polym. Sci.*, 136(2019), No. 11, art. No. e47183.

[52] N.A.M. Radzuan, M.Y. Zakaria, A.B. Sulong, and J. Sahari, The effect of milled carbon fibre filler on electrical conductivity in highly conductive polymer composites, *Composites*, *Part B*, 110(2017), p. 153.

[53] W.W. Li, S. Jing, S.B. Wang, C. Wang, and X.F. Xie, Experimental investigation of expanded graphite/phenolic resin composite bipolar plate, *Int. J. Hydrogen Energy*, 41(2016), No. 36, p. 16240.

[54] S.H. Frensch, F. Fouda-Onana, G. Serre, D. Thoby, S.S. Araya, and S.K. Kær, Influence of the operation mode on PEM water electrolysis degradation, *Int. J. Hydrogen Energy*, 44(2019), No. 57, p. 29889.

[55] K. McCay, S. Laedre, S.Y. Martinsen, G. Smith, A.O. Barnett, and P. Fortin, Communication-*in situ* monitoring of interfacial contact resistance in PEM fuel cells, *J. Electrochem. Soc.*, 168(2021), No. 6, art. No. 064514.

[56] G.Y. Liu, F.G. Hou, S.L. Peng, X.D. Wang, and B.Z. Fang, Process and challenges of stainless steel based bipolar plates for proton exchange membrane fuel cells, *Int. J. Miner. Metall. Mater.*, 29(2022), No. 5, p. 1099.

[57] P. Yi, L.J. Zhu, C.F. Dong, and K. Xiao, Corrosion and interfacial contact resistance of 316L stainless steel coated with magnetron sputtered ZrN and TiN in the simulated cathodic environment of a proton-exchange membrane fuel cell, *Surf. Coat. Technol.*, 363(2019), p. 198.

[58] J.F. Shi, P.C. Zhang, Y.T. Han, *et al*., Investigation on electrochemical behavior and surface conductivity of titanium carbide modified Ti bipolar plate of PEMFC, *Int. J. Hydrogen Energy*, 45(2020), No. 16, p. 10050.

[59] G.Q. Yang, S.L. Yu, J.K. Mo, *et al*., Bipolar plate development with additive manufacturing and protective coating for durable and high-efficiency hydrogen production, *J. Power Sources*, 396(2018), p. 590.

[60] H.H. Ghahfarokhi, A. Saatchi, and S.M. Monirvaghefi, Corrosion investigation of chromium nitride and chromium carbide coatings for PEM fuel cell bipolar plates in simulated cathode condition, *Fuel Cells*, 16(2016), No. 3, p. 356.

[61] T. Li, Z. Yan, Z.Z. Liu, Y.G. Yan, and Y.G. Chen, Surface microstructure and performance of TiN monolayer film on titanium bipolar plate for PEMFC, *Int. J. Hydrogen Energy*, 46(2021), No. 61, p. 31382.

[62] N. Rojas, M. Sánchez-Molina, G. Sevilla, *et al*., Coated stainless steels evaluation for bipolar plates in PEM water electrolysis conditions, *Int. J. Hydrogen Energy*, 46(2021), No. 51, p. 25929.

[63] P. Yi, D. Zhang, L. Peng, and X. Lai, Impact of film thickness on defects and the graphitization of nanothin carbon coatings used for metallic bipolar plates in proton exchange membrane fuel cells, *ACS Appl. Mater. Interfaces*, 10(2018), No. 40, p. 34561.

[64] S. Akula, P. Kalaiselvi, A.K. Sahu, and S. Chellammal, Electrodeposition of conductive PAMT/PPY bilayer composite coatings on 316L stainless steel plate for PEMFC application, *Int. J. Hydrogen Energy*, 46(2021), No. 34, p. 17909.

[65] Y. Wang, Y.H. Pang, H. Xu, A. Martinez, and K.S. Chen, PEM fuel cell and electrolysis cell technologies and hydrogen infrastructure development–A review, *Energy Environ. Sci.*, 15(2022), No. 6, p. 2288.

[66] D.C. Kong, C.F. Dong, X.Q. Ni, *et al*., Superior resistance to hydrogen damage for selective laser melted 316L stainless steel in a proton exchange membrane fuel cell environment, *Corros. Sci.*, 166(2020), art. No. 108425.

[67] Y. Zeng, Z. He, Q. Hua, Q. Xu, and Y. Min, Polyacrylonitrile infused in a modified honeycomb aluminum alloy bipolar plate and its acid corrosion resistance, *ACS Omega*, 5(2020), No. 27, p. 16976.

[68] H. Wakayama and K. Yamazaki, Low-cost bipolar plates of Ti_4O_7-coated Ti for water electrolysis with polymer electrolyte membranes, *ACS Omega*, 6(2021), No. 6, p. 4161.

[69] H.S. Heo and S.J. Kim, Investigation of electrochemical characteristics and interfacial contact resistance of TiN-coated titanium as bipolar plate in polymer electrolyte membrane fuel cell, *Coatings*, 13(2023), No. 1, art. No. 123.

[70] S. Lædre, O.E. Kongstein, A. Oedegaard, H. Karoliussen, and F. Seland, Materials for proton exchange membrane water electrolyzer bipolar plates, *Int. J. Hydrogen Energy*, 42(2017), No. 5, p. 2713.

[71] Y. Liu, S.B. Huang, S.L. Peng, H. Zhang, L.F. Wang, and X.D. Wang, Novel Au nanoparticles-inlaid titanium paper for PEM water electrolysis with enhanced interfacial electrical conductivity, *Int. J. Miner. Metall. Mater.*, 29(2022), No. 5, p. 1090.

[72] A.S. Gago, S.A. Ansar, B. Saruhan, *et al*., Protective coatings on stainless steel bipolar plates for proton exchange membrane (PEM) electrolysers, *J. Power Sources*, 307(2016), p. 815.

[73] E.F. Mine, Y. Ito, Y. Teranishi, M. Sato, and T. Shimizu, Surface coating and texturing on stainless-steel plates to decrease the contact resistance by using screen printing, *Int. J. Hydrogen Energy*, 42(2017), No. 31, p. 20224.

[74] Y.L. Wang, S.H. Zhang, Z.X. Lu, P. Wang, X.H. Ji, and W.H. Li, Preparation and performance of electrically conductive Nb-doped TiO_2/polyaniline bilayer coating for 316L stainless steel bipolar plates of proton-exchange membrane fuel cells, *RSC Adv.*, 8(2018), No. 35, p. 19426.

[75] Y.L. Wang, Q.Y. Tan, and B. Huang, Synthesis and properties of novel N/Ta-co-doped TiO_2 coating on titanium in simulated PEMFC environment, *J. Alloys Compd.*, 879(2021), art. No. 160470.

[76] W.J. Lee, E.Y. Yun, H.B.R. Lee, S.W. Hong, and S.H. Kwon, Ultrathin effective TiN protective films prepared by plasma-enhanced atomic layer deposition for high performance metallic bipolar plates of polymer electrolyte membrane fuel cells, *Appl. Surf. Sci.*, 519(2020), art. No. 146215.

[77] L.X. Yang, R.J. Liu, Y. Wang, H.J. Liu, C.L. Zeng, and C. Fu, Corrosion and interfacial contact resistance of nanocrystalline β-Nb_2N coating on 430 FSS bipolar plates in the simulated PEMFC anode environment, *Int. J. Hydrogen Energy*, 46(2021), No. 63, p. 32206.

[78] J.J. Ma, J. Xu, S.Y. Jiang, P. Munroe, and Z.H. Xie, Effects of pH value and temperature on the corrosion behavior of a Ta_2N nanoceramic coating in simulated polymer electrolyte membrane fuel cell environment, *Ceram. Int.*, 42(2016), No. 15, p. 16833.

[79] X.Z. Wang, T.P. Muneshwar, H.Q. Fan, K. Cadien, and J.L. Luo, Achieving ultrahigh corrosion resistance and conductive zirconium oxynitride coating on metal bipolar plates by plasma enhanced atomic layer deposition, *J. Power Sources*, 397(2018), p. 32.

[80] N. Abbas, X.D. Qin, S. Ali, *et al.*, Study of microstructural variation with annealing temperature of Ti–Al–C films coated on stainless steel substrates, *Int. J. Hydrogen Energy*, 45(2020), No. 4, p. 3186.

[81] H.Q. Fan, D.D. Shi, X.Z. Wang, J.L. Luo, J.Y. Zhang, and Q. Li, Enhancing through-plane electrical conductivity by introducing Au microdots onto TiN coated metal bipolar plates of PEMFCs, *Int. J. Hydrogen Energy*, 45(2020), No. 53, p. 29442.

[82] X.Y. Wang, L.G. Cui, J. Feng, and W. Chen, Artificial intelligence for breast ultrasound: An adjunct tool to reduce excessive lesion biopsy, *Eur. J. Radiol.*, 138(2021), art. No. 109624.

[83] P.F. Yan, T. Ying, Y.X. Li, *et al.*, A novel high corrosion-resistant polytetrafluoroethylene/carbon cloth/Ag coating on magnesium alloys as bipolar plates for light-weight proton exchange membrane fuel cells, *J. Power Sources*, 484(2021), art. No. 229231.

[84] P.P. Gao, Z.Y. Xie, X.B. Wu, *et al.*, Development of Ti bipolar plates with carbon/PTFE/TiN composites coating for PEMFCs, *Int. J. Hydrogen Energy*, 43(2018), No. 45, p. 20947.

[85] P.Y. Yi, D. Zhang, D.K. Qiu, L.F. Peng, and X.M. Lai, Carbon-based coatings for metallic bipolar plates used in proton exchange membrane fuel cells, *Int. J. Hydrogen Energy*, 44(2019), No. 13, p. 6813.

[86] X.B. Li, L.F. Peng, D. Zhang, P.Y. Yi, and X.M. Lai, The frequency of pulsed DC sputtering power introducing the graphitization and the durability improvement of amorphous carbon films for metallic bipolar plates in proton exchange membrane fuel cells, *J. Power Sources*, 466(2020), art. No. 228346.

[87] P.Y. Yi, W.X. Zhang, F.F. Bi, L.F. Peng, and X.M. Lai, Microstructure and properties of a-C films deposited under different argon flow rate on stainless steel bipolar plates for proton exchange membrane fuel cells, *J. Power Sources*, 410(2019), p. 188.

[88] A.L. Ahmad, U.R. Farooqui, and N.A. Hamid, Porous (PVDF-HFP/PANI/GO) ternary hybrid polymer electrolyte membranes for lithium-ion batteries, *RSC Adv.*, 8(2018), No. 45, p. 25725.

[89] V.A. Setyowati, H.C. Huang, C.C. Liu, and C.H. Wang, Effect of iron precursors on the structure and oxygen reduction activity of iron–nitrogen–carbon catalysts, *Electrochim. Acta*, 211(2016), p. 933.

[90] A.U. Devi, K. Divya, D. Rana, M.S. A. Saraswathi, and A. Nagendran, Highly selective and methanol resistant polypyrrole laminated SPVdF-co-HFP/PWA proton exchange membranes for DMFC applications, *Mater. Chem. Phys.*, 212(2018), p. 533.

[91] T.J. Pan, X.W. Zuo, T. Wang, J. Hu, Z.D. Chen, and Y.J. Ren, Electrodeposited conductive polypyrrole/polyaniline composite film for the corrosion protection of copper bipolar plates in proton exchange membrane fuel cells, *J. Power Sources*, 302(2016), p. 180.

[92] X.J. Liu, T. Wu, Z.X. Dai, *et al.*, Bipolarly stacked electrolyser for energy and space efficient fabrication of supercapacitor electrodes, *J. Power Sources*, 307(2016), p. 208.

[93] Y.L. Wang, S.H. Zhang, P. Wang, Z.X. Lu, S.B. Chen, and L.S. Wang, Synthesis and corrosion protection of Nb doped TiO_2 nanopowders modified polyaniline coating on 316 stainless steel bipolar plates for proton-exchange membrane fuel cells, *Prog. Org. Coat.*, 137(2019), art. No. 105327.

[94] G.Y. Liu, F.G. Hou, X.D. Wang, and B.Z. Fang, Conductive polymer and nanoparticle-promoted polymer hybrid coatings for metallic bipolar plates in proton membrane exchange water electrolysis, *Appl. Sci.*, 13(2023), No. 3, art. No. 1244.

[95] S. Almheiri and H.T. Liu, Direct measurement of methanol crossover fluxes under land and channel in direct methanol fuel cells, *Int. J. Hydrogen Energy*, 40(2015), No. 34, p. 10969.

[96] L.Z. Wu, L. An, D.K. Jiao, Y.F. Xu, G.B. Zhang, and K. Jiao, Enhanced oxygen discharge with structured mesh channel in proton exchange membrane electrolysis cell, *Appl. Energy*, 323(2022), art. No. 119651.

[97] X.Y. Zhang, B.W. Wang, Y.F. Xu, *et al.*, Effects of different loading strategies on the dynamic response and multi-physics fields distribution of PEMEC stack, *Fuel*, 332(2023), art. No. 126090.

[98] Z.M. Bao, Z.Q. Niu, and K. Jiao, Analysis of single- and two-phase flow characteristics of 3-D fine mesh flow field of proton exchange membrane fuel cells, *J. Power Sources*, 438(2019), art. No. 226995.

[99] G.B. Zhang, X. Xie, B. Xie, Q. Du, and K. Jiao, Large-scale multi-phase simulation of proton exchange membrane fuel cell, *Int. J. Heat Mass Transf.*, 130(2019), p. 555.

[100] F. Aubras, J. Deseure, J.J.A. Kadjo, *et al.*, Two-dimensional model of low-pressure PEM electrolyser: Two-phase flow regime, electrochemical modelling and experimental validation, *Int. J. Hydrogen Energy*, 42(2017), No. 42, p. 26203.

[101] S. Park, W. Lee, and Y. Na, Performance comparison of proton exchange membrane water electrolysis cell using channel and PTL flow fields through three-dimensional two-phase flow simulation, *Membranes*, 12(2022), No. 12, art. No. 1260.

[102] L.Z. Wu, G.B. Zhang, B. Xie, C. Tongsh, and K. Jiao, Integration of the detailed channel two-phase flow into three-dimensional multi-phase simulation of proton exchange membrane electrolyzer cell, *Int. J. Green Energy*, 18(2021), No. 6, p. 541.

[103] E. Hontañón, M.J. Escudero, C. Bautista, P.L. García-Ybarra, and L. Daza, Optimisation of flow-field in polymer electrolyte membrane fuel cells using computational fluid dynamics techniques, *J. Power Sources*, 86(2000), No. 1-2, p. 363.

[104] A. Kumar and R.G. Reddy, Effect of channel dimensions and shape in the flow-field distributor on the performance of polymer electrolyte membrane fuel cells, *J. Power Sources*, 113(2003), No. 1, p. 11.

[105] Y.H. Lu and R.G. Reddy, Performance of micro-PEM fuel

cells with different flow fields, *J. Power Sources*, 195(2010), No. 2, p. 503.
[106] S.Y. Zhang, H.T. Xu, Z.G. Qu, S. Liu, and F.K. Talkhoncheh, Bio-inspired flow channel designs for proton exchange membrane fuel cells: A review, *J. Power Sources*, 522(2022), art. No. 231003.
[107] M. Sauermoser, B.G. Pollet, N. Kizilova, and S. Kjelstrup, Scaling factors for channel width variations in tree-like flow field patterns for polymer electrolyte membrane fuel cells-An experimental study, *Int. J. Hydrogen Energy*, 46(2021), No. 37, p. 19554.
[108] P. Trogadas, J.I.S. Cho, T.P. Neville, *et al*., A lung-inspired approach to scalable and robust fuel cell design, *Energy Environ. Sci.*, 11(2018), No. 1, p. 136.
[109] A. Ghanbarian and M.J. Kermani, Enhancement of PEM fuel cell performance by flow channel indentation, *Energy Convers. Manage.*, 110(2016), p. 356.
[110] Y. Yin, S.Y. Wu, Y.Z. Qin, O.N. Otoo, and J.F. Zhang, Quantitative analysis of trapezoid baffle block sloping angles on oxygen transport and performance of proton exchange membrane fuel cell, *Appl. Energy*, 271(2020), art. No. 115257.
[111] Y.L. Wang, X.A. Wang, Y.Z. Fan, W. He, J.L. Guan, and X.D. Wang, Numerical investigation of tapered flow field configurations for enhanced polymer electrolyte membrane fuel cell performance, *Appl. Energy*, 306(2022), art. No. 118021.
[112] C.J. Xu, H. Wang, and T.H. Cheng, Wave-shaped flow channel design and optimization of PEMFCs with a groove in the gas diffusion layer, *Int. J. Hydrogen Energy*, 48(2023), No. 11, p. 4418.
[113] X.C. Meng, H. Ren, F. Xie, and Z.G. Shao, Experimental study and optimization of flow field structures in proton exchange membrane fuel cell under different anode modes, *Int. J. Hydrogen Energy*, 48(2023), No. 63, p. 24447.
[114] G. Zhang, Z. Qu, W.Q. Tao, *et al*., Porous flow field for next-generation proton exchange membrane fuel cells: Materials, characterization, design, and challenges, *Chem. Rev.*, 123(2023), No. 3, p. 989.
[115] Q. Wei, L.X. Fan, and Z.K. Tu, Hydrogen production in a proton exchange membrane electrolysis cell (PEMEC) with titanium meshes as flow distributors, *Int. J. Hydrogen Energy*, 48(2023), No. 93, p. 36271.
[116] G.B. Zhang, Z.G. Qu, and Y. Wang, Proton exchange membrane fuel cell of integrated porous bipolar plate–gas diffusion layer structure: Entire morphology simulation, *eTransportation*, 17(2023), art. No. 100250.
[117] Y. Nonobe, Development of the fuel cell vehicle mirai, *IEEJ Trans. Electr. Electron. Eng.*, 12(2017), No. 1, p. 5.
[118] C. Sun, Y. Wang, M.D. McMurtrey, N.D. Jerred, F. Liou, and J. Li, Additive manufacturing for energy: A review, *Appl. Energy*, 282(2021), art. No. 116041.
[119] X. He, D.C. Kong, Y.Q. Zhou, *et al*., Powder recycling effects on porosity development and mechanical properties of Hastelloy X alloy during laser powder bed fusion process, *Addit. Manuf.*, 55(2022), art. No. 102840.
[120] Y.F. Xu, G.B. Zhang, L.Z. Wu, Z.M. Bao, B.F. Zu, and K. Jiao, A 3-D multiphase model of proton exchange membrane electrolyzer based on open-source CFD, *Digit. Chem. Eng.*, 1(2021), art. No. 100004.
[121] G.J. Chen, W.D. Shi, J. Xuan, *et al*., Improvement of under-the-rib oxygen concentration and water removal in proton exchange membrane fuel cells through three-dimensional metal printed novel flow fields, *AlChE. J.*, 68(2022), No. 9, art. No. e17758.
[122] G.Q. Yang, J.K. Mo, Z.Y. Kang, *et al*., Fully printed and integrated electrolyzer cells with additive manufacturing for high-efficiency water splitting, *Appl. Energy*, 215(2018), p. 202.
[123] G.Q. Yang, S.L. Yu, Z.Y. Kang, *et al*., A novel PEMEC with 3D printed non-conductive bipolar plate for low-cost hydrogen production from water electrolysis, *Energy Convers. Manage.*, 182(2019), p. 108.
[124] G.Q. Yang, Z.Q. Xie, S.L. Yu, *et al*., All-in-one bipolar electrode: A new concept for compact and efficient water electrolyzers, *Nano Energy*, 90(2021), art. No. 106551.
[125] J.E. Park, J. Lim, M.S. Lim, *et al*., Gas diffusion layer/flow-field unified membrane-electrode assembly in fuel cell using graphene foam, *Electrochim. Acta*, 323(2019), art. No. 134808.
[126] X.C. Wang, H.L. Ma, H.Q. Peng, *et al*., Enhanced mass transport and water management of polymer electrolyte fuel cells via 3-D printed architectures, *J. Power Sources*, 515(2021), art. No. 230636.
[127] A. Kopanidis, A. Theodorakakos, E. Gavaises, and D. Bouris, 3D numerical simulation of flow and conjugate heat transfer through a pore scale model of high porosity open cell metal foam, *Int. J. Heat Mass Transf.*, 53(2010), No. 11-12, p. 2539.
[128] L. Wei, A.M. Dafalla, and F.M. Jiang, Effects of reactants/coolant non-uniform inflow on the cold start performance of PEMFC stack, *Int. J. Hydrogen. Energy*, 45(2020), No. 24, p. 13469.
[129] J. Choi and G. Son, Numerical study of droplet motion in a microchannel with different contact angles, *J. Mech. Sci. Technol.*, 22(2008), No. 12, p. 2590.
[130] L.M. Pant, S.K. Mitra, and M. Secanell, Absolute permeability and Knudsen diffusivity measurements in PEMFC gas diffusion layers and micro porous layers, *J. Power Sources*, 206(2012), p. 153.
[131] S. Lee, T. Kim, and H. Park, Comparison of multi-inlet and serpentine channel design on water production of PEMFCs, *Chem. Eng. Sci.*, 66(2011), No. 8, p. 1748.